# Comparison of Lift & Drag of Different Bird Wings by Numerical Analysis

*A Thesis Submitted to*

**Department of Mechanical and Production Engineering**

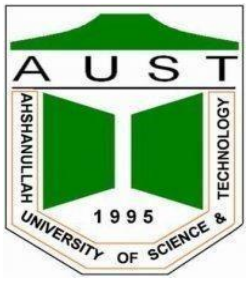


**Ahsanullah University of Science and Technology**

*By*

**Omar Saif** **[13-02-08-035]**

**Md. Tanvir Nasir** **[14-01-08-014]**

**Md. Touqir Ahsan** **[14-01-08-048]**

*Under the Supervision of*

**Fazlar Rahman**

In partial fulfillment of the requirement for the degree of

**Bachelor of Science in Mechanical Engineering**

# Acknowledgement

First and foremost, we are grateful to almighty Allah for all His blessings. We would like to acknowledge Dept. of Mechanical and Production Engineering of Ahsanullah University of Science and Technology for such a wonderful opportunity and environment for conducting the research.

We would like to extend our sincerest appreciation to the thesis supervisor, Fazlar Rahman. He is a great mentor whose expert opinions and guidance have been central to the success of completion of the initial phase of the thesis. Working with him has been both enjoyable and a learning experience. His expert's suggestions on our testing and designing helped us to save a lot of time and cost with full confidence.

Finally, we would like to express our deepest gratitude to everyone in our family, especially our loving parents who have been very kind and understanding throughout. We owe a lot of respect to them for their fabulous upbringing. We wouldn't be here without their sincerest support and motivation.

We are honored and privileged to be surrounded and helped by people and opportunities like mentioned.

# Abstract

Aircraft performance is highly affected by induced drag caused by wing vortices. Many types of wings have been designed and their significance in reducing drag is published.

Understanding the gliding position of various long voyager and hunter birds is the critical step of our thesis, as we are opting to implement the geometry and positioning of the wings subjected to this flight pattern to a traditional commercial airliner –specifically the Boeing 787-800 Dreamliner. Minimized induced drag and maximized vertical lift is the reason why gliding is an attractive flight strategy. Implementing this should yield a better aerodynamic performance over the traditional wing design. Note that, the airfoil cross section remains constant for all the wing shapes. The only variable is the plane geometry of the wings. Primarily, a scale of 172.5:1 is taken into account for this thesis. The CAD designs are done and various mass and surface area properties are calculated via Solid works. All the wings are approximately 157 mm long, with sliding slots taken into account. All the wings and the mount are 3D printed with plastic. The constructions are then fitted to a subsonic wind tunnel and then tested for drag and lift force in various angle of attacks, which were controlled by the mount rod. An analytical study via computer simulations is also done for validation by ANSYS Fluent Simulation.

# Table of Contents

# NOMENCLETURE

| | | | |
|---|---|---|---|
| A | projected area | x | streamwise coordinate [m] |
| B | additive constant | y | transverse coordinate [m] |
| $C_d$ | drag coefficient | $\mu$ | dynamic viscosity [$Nsm^{-2}$] |
| $C_l$ | lift coefficient | $\mu_t$ | eddy viscosity [$Nsm^{-2}$] |
| F | force | $\alpha$ | angle of attack [degree] |
| S | surface area [$mm^2$] | k | turbulent kinetic energy[$m^2s^{-2}$] |
| P | pressure [$Nm^2$] | $\rho$ | density [$kgm^{-3}$] |
| $R_e$ | Reynolds number | V | speed [m/s] |
| T | temperature [K] | $\epsilon$ | specific dissipation [$s^{-1}$] |

# List of Figures

**Figure No.** **Page No.**

Figure 50: Wing located in the center of the 3D domain in ANSYS.

Figure 51: Mesh around the wing.

Figure 52: Setup chart in ANSYS 17

Figure 53: NACA 2451 airfoil cross section

# List of Tables

**Table/Graph No.** **Page No.**

# Introduction

Since at least the myth of Icarus, wings seen in nature have inspired humanity's dreams of flight. In the more than a century since the Wright brothers flew the first airplane, Flyer 1, people have begun making these fantasies a reality, flying high enough above the Earth to make it all the way to the moon. However, in many ways, nature still has much to teach aircraft designers. For instance, while airplanes now often break the sound barrier, their stiff wings limit their performance. The following are just a few of the nature inspired improvements in aviation engineering and technology.

Figure 1: Juan lacruz


Figure 2: Bombardier

When birds come in for a landing, they execute a series of maneuvers and adjustments that allow them to make extremely accurate stops on difficult perches. Birds do not use the standard, linear landings made by most aircraft. Engineers are testing how to recreate bird-like adjustments in speed and direction to help aircraft land safely and accurately. The aircraft of the future may not need runways or brakes! Bird morphing wings and perching behaviors that are influencing aviation design are discussed in the 2011 abstract by Elvin Pineda from the University of Massachusetts.

## 1.1 Gliding Flight

Gliding flight is a common flight style in birds that tends to hunt preys and embarks upon longer voyages. The reason for this is that it enables them to maximize lift by extending their wings to the fullest and technically max out the projected areas casted by the wings. This is a very efficient way to wander around where not a lot of induced drag is generated. Studying this

phenomenon is the key to our research as we are opting to minimize induced drag and maximize lift.

Since the dawn of time, mankind has struggled in various practical and engineering applications. And more than we know, natural elements came to the rescue. Studying the nature and implementing the outcomes, results and designs to engineering problems has always been a viable approach. The Wright brothers were inspired by pigeons before becoming the first human beings to fly. During World War II, a lot of historic German designs were influenced by natural elements. Superbikes these days have somewhat implications and designing elements directly influenced by fast animals like Cheetahs, Panthers and so on. This trend is known as bionic engineering.

Figure 3: A wandering albatross in a gliding flight position.

## 1.2 Birds Selection

Basically, 3 different birds have been selected for this thesis. Each representing a specific class of birds, these are –

1. Swift, representing agile and fast birds
2. Falcon, representing hunter birds that specialize in diving
3. Wandering Albatross, representing long voyaging gliders

Using the same airfoil cross section, the wings are designed – inspired by the wing geometry of these birds while they are in gliding position. Solid works was used to design 3D CAD models of the scaled wings. Upon completing CAD designs, mass properties, surface areas and other physical characteristics are calculated using evaluation tools of Solid works. The manufacturing method was 3D printing.

The thesis is parted in three different phases. These are

1. Single Wing Test – Primary Phase
2. Full Body Test – Secondary Phase
3. Computer Simulations – Analysis Phase

The following is a graphical overview of the birds and 3D models of their corresponding wing shapes –

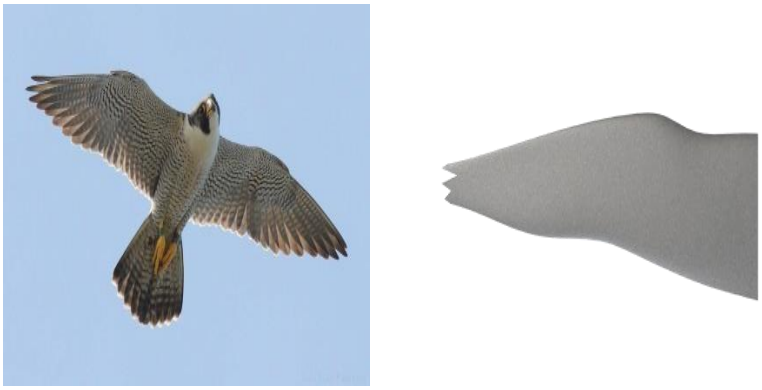

Figure 4: Falcon Wing

Figure 5: Swift Wing

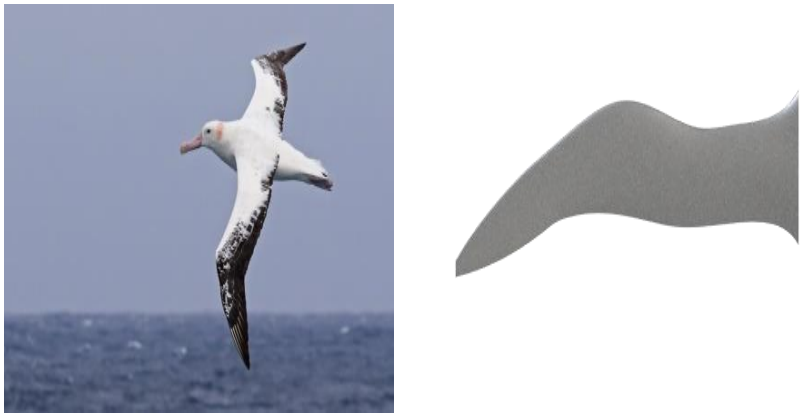

Figure 6: Wandering Albatross Wing

## 1.3 Drag Force

Drag is the force experienced by an object representing the resistance to its movement through a fluid. Sometimes called wind resistance or fluid resistance, it acts in the opposite direction to the relative motion between the object and the fluid. The figure below shows the aerodynamics drag forces experienced by an airfoil or aircraft wing moving through the air with constant angle of attack as the air speed is increased. There are different types of drag in aerodynamics. The graphical representation of different drag for different air velocity in shown in Figure 10.

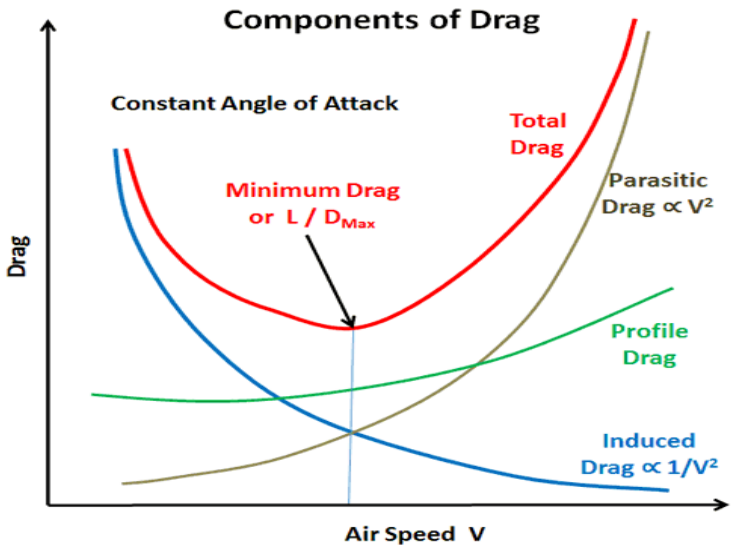


Figure 7: Drag vs Air speed.

The total aerodynamics drag is the sum of the following components:

- **Induced drag** – Due to the vortices and turbulence resulting from the running of the air flow and downwash associated with the generation of lift. Increases with the angle of attack. Inversely proportional to the square of the air speed. Decrease as aircraft speed increases and the angle of attack is reduced.
- **Wave drag** - In aeronautics, wave drag is a component of the aerodynamic drag on aircraft wing and fuselage propeller blade tips and projectiles moving at transonic and supersonic speeds, due to the presence of shock waves. Wave drag is

independent of viscous effects, and tends to present itself as a sudden and dramatic increase in drag as the vehicle increases speed to the Critical Mach number. It is the sudden and dramatic rise of wave drag that leads to the concept of a sound barrier.

- **Friction drag-** Arises from the friction of the air against the "skin" of the airfoil moving through it. Increases with the surface area of the airfoil and the square of air speed.

- **Profile drag or Viscous Drag** - The sum of **Friction Drag** and the **Form drag.**

- **Parasitic Drag** - Parasitic drag is drag that results when an object is moved through a fluid medium. In the case of aerodynamic drag, the fluid medium is the atmosphere. Parasitic drag is a combination of form drag, skin friction drag and interference drag.

## 1.4 Lift Force

Lift is the force that directly opposes the weight of an airplane and holds the airplane in the air. Lift is generated by every part of the airplane, but most of the lift on a normal airliner is generated by the wings. Lift is a mechanical aerodynamic force produced by the motion of the airplane through the air. Because lift is a force, it is a vector quantity, having both a magnitude and a direction associated with it. Lift acts through the center of pressure of the object and is directed perpendicular to the flow direction. There are several factors which affect the magnitude of lift.

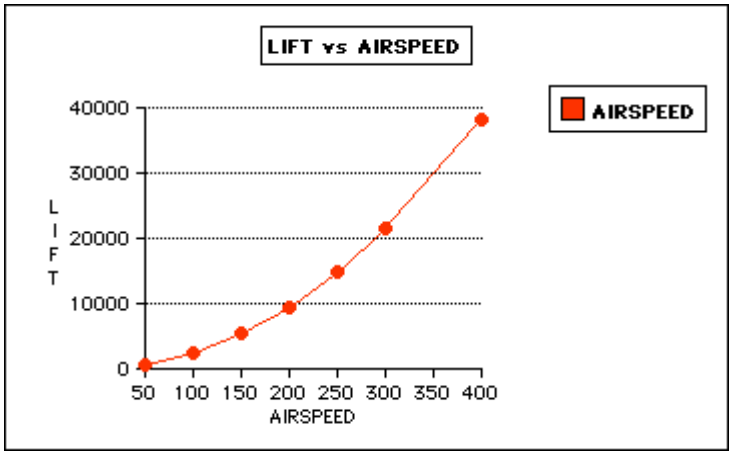


Figure 8: Lift vs Air speed.

Lift occurs when a moving flow of gas is turned by a solid object. The flow is turned in one direction, and the lift is generated in the opposite direction, according to Newton's Third Law of action and reaction. Because air is a gas and the molecules are free to move about, any solid surface can deflect a flow. For an aircraft wing, both the upper and lower surfaces contribute to the flow turning. Neglecting the upper surface's part in turning the flow leads to an incorrect theory of lift.

**NO fluid, NO** Lift is a mechanical force. It is generated by the interaction and contact of a solid body with a fluid (liquid or gas). It is not generated by a force field, in the sense of a gravitational field, or an electromagnetic field, where one object can affect another object without being in physical contact. For lift to be generated, the solid body must be in contact with the fluid: no fluid, no lift. The Space Shuttle does not stay in space because of lift from its wings but because of orbital mechanics related to its speed. Space is nearly a vacuum. Without air, there is no lift generated by the wings.

**NO motion, NO** Lift is generated by the difference in velocity between the solid object and the fluid. There must be motion between the object and the fluid: no motion, no lift. It makes no difference whether the object moves through a static fluid, or the fluid moves past a static solid object. Lift acts perpendicular to the motion. Drag acts in the direction opposed to the motion.

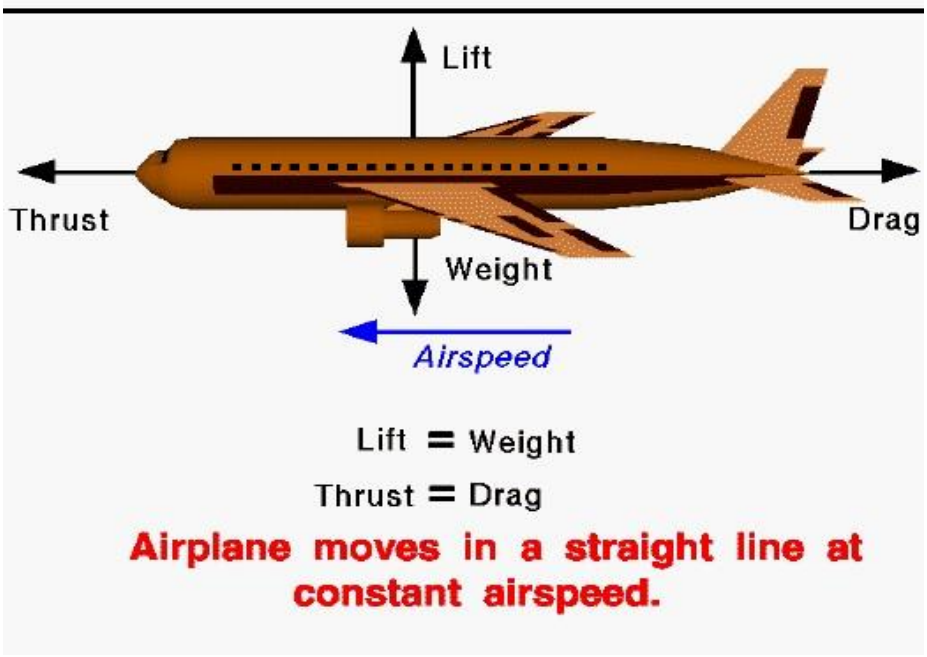


Figure 9: Lift of an Airplane.

## 1.5 Flow over Sphere

A flow separation around rigid spherical is an undesirable flow feature in many engineering applications. The separation angle is important because they control the size of the form loss and drag force created by the wakes at the rear of the tubes. This flow causes increases of drag, loss of lift, diminished pressure recovery which gives hurdles to such application. As drag estimates to a large amount, the running costs of transport of fluids, drag reduction is a crucial design issue in engineering. Therefore, a lot of attention is given by researchers to control the flow separation.

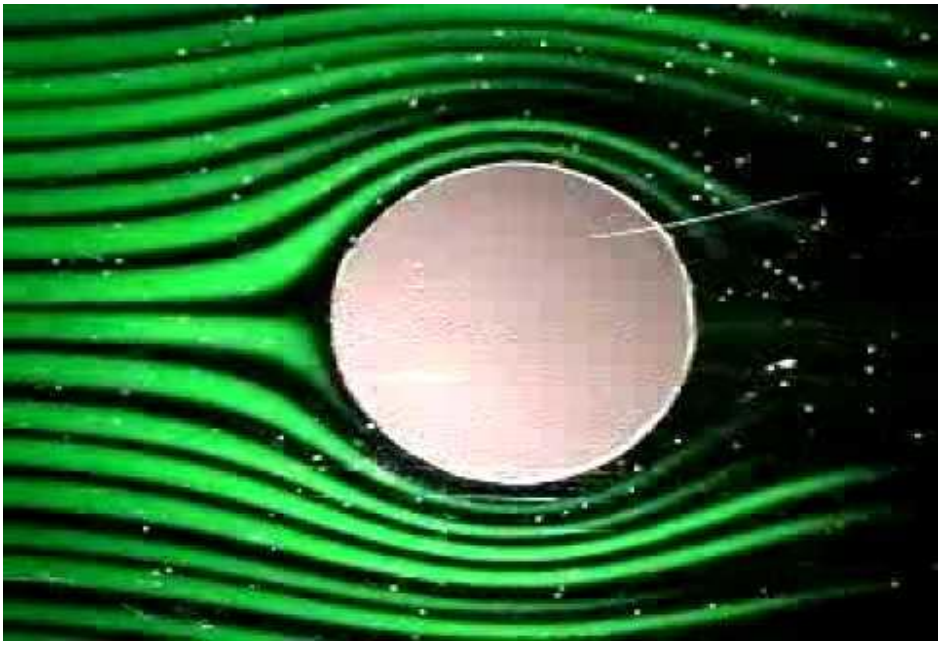

Figure 10: Laminar flow over a Sphere.

Special attention is given to unsteady phenomena in aerodynamic & hydrodynamic. The flows around the sphere as flow over a ball shown in Figure 13, the stability of the wake, the possible flow separation or boundary layer separation that occur behind the sphere, affect significantly the mass, momentum and energy transfer and determine the values of the transport coefficient. The visualization study by wave shown that the fluid flow is attached to the sphere and there is no visible recirculation behind it at ($0 \leq Re \leq 20$). This is called attached flow region. Both theoretical arguments and experimental velocity measurement demonstrate that there is a velocity defect region behind the sphere as shown as Figure 14, which is the characteristic of a weak and stable wake. In this flow regime, the flow is attached on the surface of the sphere and the separation does not occur. The pressure and the characteristic of the wake re noticeable in the asymmetry of the vortices filed and to a lesser extent, the a symmetry of the streamline counters.

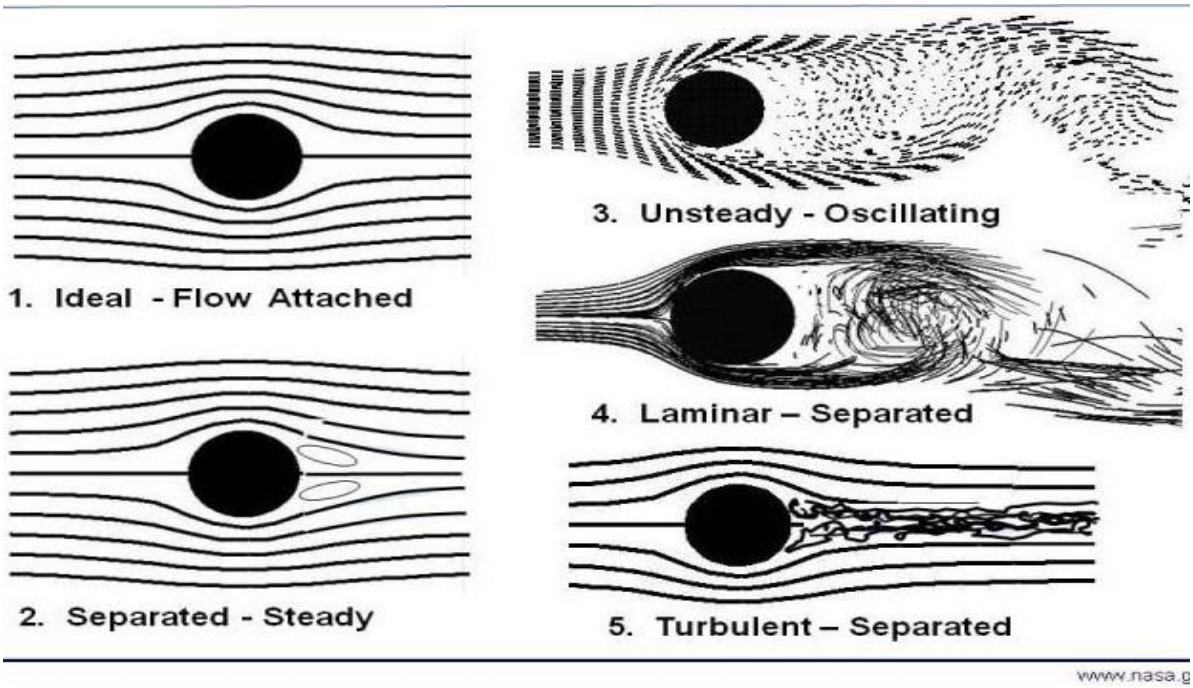


Figure 11: Flow over Sphere with gradual increase of velocity and Reynolds number.

In a steady- state wake region ($20 \leq Re \leq 210$), the wake become, wider and longer and its point of attachment on the sphere moves forward, as the value of Reynolds number increases. The separation angle for the wake, which starts at $180^{\circ}$ at Re = 20 decreases monotonically with increasing Re to a value of approximately $120^{\circ}$ at Re = 130. Above the transition flow ($210 \leq Re \leq 270$), where at point near Re = 210, noted that the flow remained attached and stable but was no longer axisymmetric. The natural of the flow in this regime consists of two streamwise vorticial tail of equal strength opposite sign. The flow becomes unsteady flow ($270 \leq Re \leq 1000$) as the Reynolds number increases.

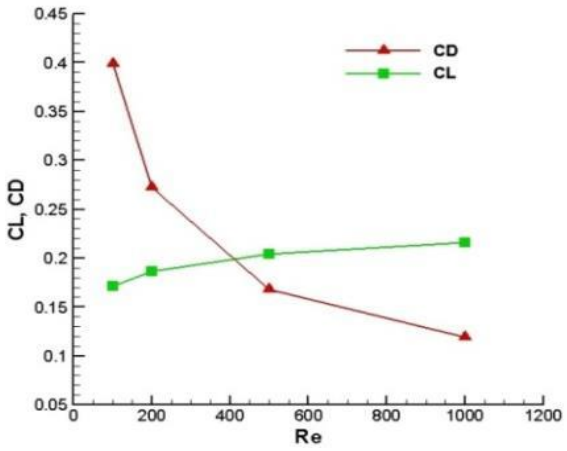


Figure 12: CL & CD of sphere with increase of Reynolds number.

## 1.6 Flow over Simple Airfoil

**Airfoils** are two- dimensional representation of three- dimensional wings. Two- dimensional airfoils can be considered the building blocks of a wing, meaning the aerodynamic characteristics of airfoils are useful for interpreting the performance of the whole wing. Figure 16 shows different parameters of a typical airfoil profile.

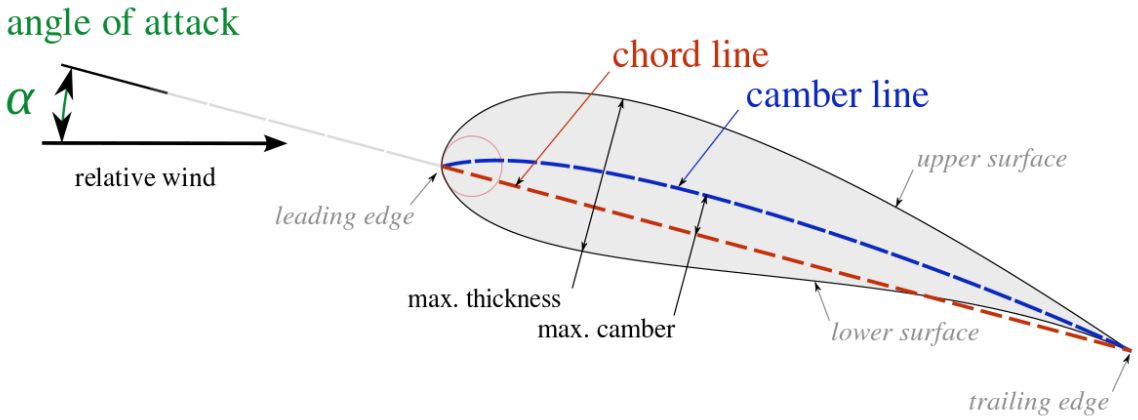


**Figure 13**: Airfoil profile nomenclature.

## 1.7 Flow over Wing

The wing is so shaped that the air on the top of the wing travels much faster than the bottom of the wing. This is achieved by curving the upper part of the wing to cover more distance than the bottom part for the same width. When wind travels above and below the wing, it needs to cover a greater distance on the top compared to the bottom in the same time. Hence the speed of the wind above would be faster than the bottom. Now, when wind travels parallel to a surface, and is faster on the top than on the bottom, the pressure on the top would turn out to be lower than the bottom. So, essentially, the pressure beneath the wing is greater than the top, causing the LIFT. This lifts the plane up and helps it stay in the air.

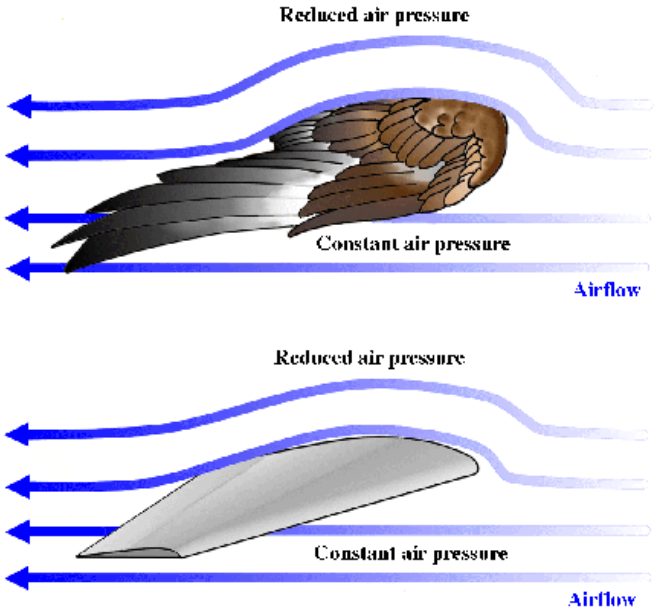


Figure 14: Comparison between bird wing with aircraft wing.

## 1.8 Coefficient of Lift ($C_l$)

Coefficient of lift or lift coefficient is a dimensionless coefficient that relates the lift generated by a lifting body to the fluid density around the body, the fluid velocity and an associated reference area. $C_l$ is a function of the angle of the body to the flow, its
Reynolds number and it's Mach number. The lift coefficient is defined by –

$$C_l = L/qS = 2L/\rho u^2 S$$

Where **L** is the lift force, **S** is the relevant surface area, and **q** is the fluid dynamic pressure.

## 1.9 Coefficient of Drag ($C_d$)

Coefficient of drag or drag coefficient is a dimensionless quantity that is used to quantify the drag or resistance of an object in a fluid environment such as water or air. $C_d$ is always associated with a particular surface area. $C_d$ is denoted as –

$$C_d = 2D/\rho u^2 S$$

Where **D** is the drag force and all the other notions have their usual meaning as mentioned.

## 1.10 Angle of Attack (α)

In fluid dynamics, angle of attack (AOA) is the angle between a reference line on a body (often the chord line of an airfoil) and the vector representing the relative motion between the body and the fluid through which it is moving.

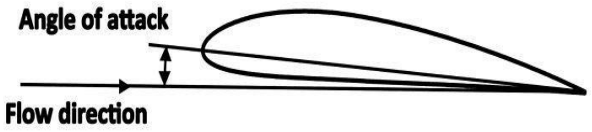


Figure 15: Angle of Attack.

The main reason to implement these geometric shapes in this particular flight pattern is to reduce drag while increase lift in such way that surpasses the traditional wing shapes commercial airliners use these days. The key here is to experiment on different wings to yield drag and lift force for different angle of attacks (AOA) and compare them with traditional wing shapes. With these results, usually a graph is plotted showing coefficient of lift ($C_l$) and coefficient of drag ($C_d$) with varying AOAs. There are a couple of things included in these graphs:

1. **Critical Angle:** The Angle where max lift is generated
2. **Stall:** It's the phase where the body will come at rest regarding generating lift

Point to be noted, stall occurs while the airfoil reaches critical angle.

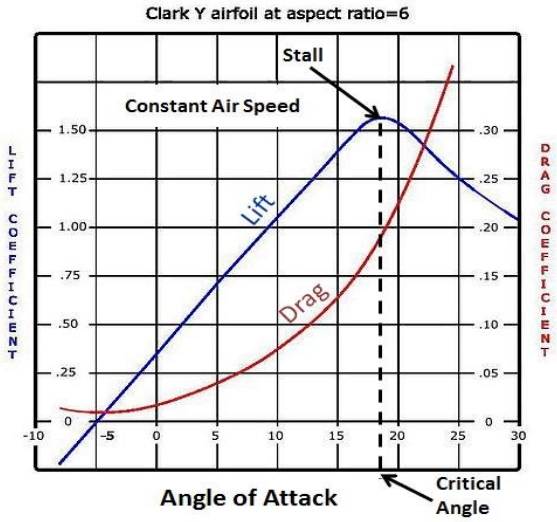


Figure 16: $C_l$ and $C_d$ for varying AOA.

# Chapter 2

## LITERATURE REVIEW

- Tobalske and Biewener, in press; Askew and Ellerby showed that many birds use non flapping phases to modulate power.

- Breat Douglas R. Warrick research about Aerodynamics of intermittent bounds in flying birds.

- Rayner, 1985 hypothesized that small birds were constrained by their muscle physiology to use a narrow range of contractile velocity in their pectoralis.

- Bret, Jason and Douglus states that $C_l$ and $C_d$ both decreased as a function of increasing flight speed and hence Re. $C_d$ decreased from .77 to .17 and Re increased from 35000 to 85000.

- Evans MR shows that birds tail do act like delta wings but delta wing theory doesn't always predict the forces they generate.

- Ryner and Ellington show that, when a wing produces a lift, there's a net circulation of air about the wing that represents the bound vortex of the wing.

# Chapter 3

## Objective

The objectives of the current research are –

- Determine the Drag & Lift of different bird wings.
- Results will be validated by Finite Element Analysis.
- Compare the result with Drag & Lift of scaled (172.5:1) model of Boeing 787-800 Aircraft wing.
- Feasibility of implementing other birds wing in Boeing 787-800.

# Chapter 4

## Bio-inspiration

In the biological world many creatures, such as bees and butterflies, use lightweight, active skeletal structures for a variety of purposes. These examples have inspired Airbus to consider the use of such “bionic structures” as part of future aircraft structures. If the aerodynamic surfaces could be made lighter or more adaptive to the local environment, the weight of the aircraft could be reduced, which would result in reduced emissions. Airbus engineers are also exploring nature-inspired manufacturing techniques to create “bionic bones”, which may enable such lightweight active structures on the aircraft of tomorrow. The Wright brothers’ warping wings went out of style once airplanes got faster. Wood-and-canvas wings fare poorly at high speeds, so engineers substituted stiffer materials, which required wings with hinged flaps.

Still, the kind of flexible wings seen in nature have long tantalized scientists for the benefits they can provide. Birds and bats can greatly vary the shape of their wings, helping them rapidly switch between a variety of tasks in complex environments. For instance, falcons can save energy loitering aloft until they see prey, at which point they can adopt a strike configuration to swoop downwards, adjusting their wings at the last second to help them deftly capture desperately junking prey.

Although stiff aircraft wings are each designed for optimal flight at one speed and one angle of attack—the angle between the wing and the direction of the airflow—they do not behave as well at other speeds or angles of attack. For example, commercial airliners have wings that sweep moderately toward the rear, while the wings of many jet fighters sweep much farther back to enable supersonic speed.

## 4.1 Shark skin

Flying creatures are not the only natural teachers that are schooling modern aviation engineers. Sharks have a groovy skin that allows them to glide through the water with the greatest of ease. Engineers copy these grooves in the hull design of aircraft in order to reduce wind drag and increase speed and efficiency.

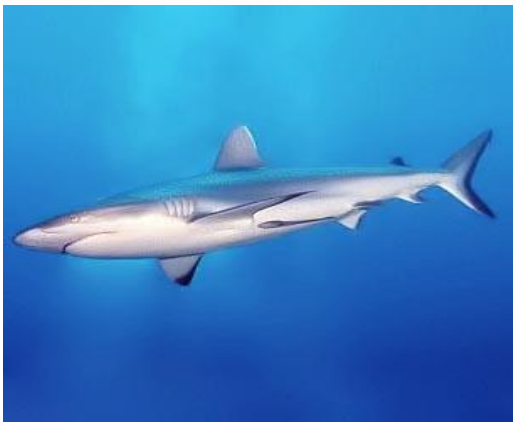

Figure 18: Harryemi shark

Figure 19: Boeing 767-300

## 4.2 Noise Reduction

Engineers are on a constant quest to reduce airplane noise. A number of creatures are giving lessons on how to keep the flying machines from disturbing the peace. The pistol shrimp emits a loud crack sound to stun prey and confuse predators while tuning the frequency out of his own brain. Bees position their honeycombs in a certain way to dampen sound. Owls are experts of stealth and silent flight. Engineers are also taking a close look at creatures such as cicadas, butterflies, and fish to provide some insight on how to develop potential noise reduction technology. Some of the ideas include retractable brush fringe and serrated engine casings.

## 4.3 Moveable wing surfaces

**Sea birds** have the ability to sense gust loads in the air with their beaks and react by adjusting the shape of their wing feathers to suppress lift. The nose of the new Airbus A350XWB contains probes which can detect gusts and deploy moveable wing surfaces for more efficient flight. This helps reduce fuel consumption and emissions.


Figure 20: A350-800 Airbus.

## 4.4 Eagle inspired winglets

If the wings of large birds like the **Steppe Eagle** were too long, their turning circle would be too big to fit inside the rising columns of warm air which they use to soar. The eagle's wings perfectly balance maximum lift with minimum length by curling feathers up at the tips until they are almost vertical. This provides a barrier against the vortex for highly efficient flight. If built to a conventional design, the A380's wingspan would have been three meters too long for the world's airports. But thanks to small devices known as 'winglets,' which mimic the upward curl of the eagle's feathers, the A380's wings are in compliance with airport limits by 20 cm. but still provide enough lift for the world's largest passenger aircraft to fly efficiently – saving fuel, lowering emissions and reducing airport congestion.


Figure 21: Airbus A380.

## 4.5 Kingfisher

It’s no surprise when we see extremely delicate wing shapes for different birds for different purposes. For instance, Japan is well known for the efficiency of its trains. The Shinkansen is the high-speed train system, and its 700 series design was directly inspired by the Kingfisher


Figure 22: Shinkansen 700 series with Kingfisher.

One of the most common flight strategies for birds (especially voyagers and hunters) is the gliding position. This way, birds extend their wings to the length of their entire wingspan to wander around and balance themselves without too much effort. This is a very effective strategy as it requires almost no energy.

# Chapter 5

## FLUID-STRUCTURE INTERACTION

Fluid-structure interaction (FSI) is a Multiphysics coupling between the laws that describe fluid dynamics and structural mechanics. This phenomenon is characterized by interactions which can be stable or oscillatory between a deformable or moving structure and a surrounding or internal fluid flow.

When a fluid flow encounters a structure, stresses and strains are exerted on the solid object forces that can lead to deformations. These deformations can be quite large or very small, depending on the pressure and velocity of the flow and the material properties of the actual structure.

Any change in the structure, such as vibration, deformation or movement due to aerodynamic forces, falls under fluid-structure interaction (FSI) analysis. There are two types of FSI: one-way FSI and two-way FSI. One-way FSI changes the fluid's behavior due to change in structure by controlled deformation, displacement or vibration. Two-way FSI is defined as changes in the structure because of aerodynamic forces and, then, a change in the aerodynamic behavior due to the changes in the surface structure caused by the flow itself.

Bird wings are flexible, and the airfoil profile changes with aerodynamic forces and flight conditions. Therefore, the study of FSI is significant to understand its impact on flight performance. For instance, fluid–structure interactions are a crucial consideration in the design of many engineering systems, e.g. aircraft, engines and bridges. Failing to consider the effects of oscillatory interactions can be catastrophic, especially in structures comprising materials susceptible to fatigue. Tacoma Narrows Bridge (1940), the first Tacoma Narrows Bridge, is probably one of the most infamous examples of large-scale failure. Aircraft wings and turbine blades can break due to FSI oscillations. Fluid–structure interaction has to be taken into account for the analysis of aneurysms in large arteries and artificial heart valves. A reed actually produces sound because the system of equations governing its dynamics has oscillatory solutions. The dynamic of reed valves used in two strokes engines and compressors is governed by FSI. The act of "blowing a raspberry" is another such example.

Fluid–structure interactions also occur in moving containers, where liquid oscillations due to the container motion impose substantial magnitudes of forces and moments to the container structure that affect the stability of the container transport system in a highly adverse manner

# Chapter 6

## Mathematical Modeling

### 6.1 Theory of Lift and Drag

Lift is the force that directly oppose the weight of an aircraft and holds the aircraft in the air. It is generated by every part of the aircraft, but most of the lift is generated by the wings. This force acts through the center of pressure of he object and is directed perpendicular to the flow direction. The flow turning theory is used to demonstrate airflow about the airfoil generating lift. Due to the airfoil geometry, the viscosity of an airflow and the Coanda effect, the airflow passes over the upper surface and creates a vertical velocity of airflow past the trailing edge show in the Figure 28. As the airfoil bends the airflow near the upper surface, it pulls on the air above it and system to form over the airfoil, creating a force called lift.

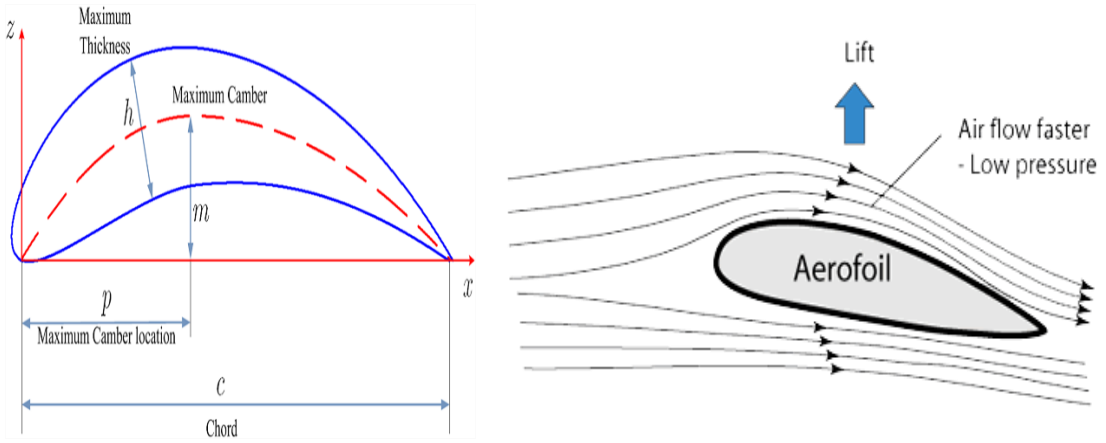


(a) (b)

Figure 23: a) Sketching of airfoil b) Airflow about the airfoil generating lift.

From Kutta-Joukowski theorem, lifting force for an airfoil with round leading and sharp trailing edge immersed in a uniform stream with an effective angle of attack, proportional to the density of air, relative velocity of the airflow and the airflow and the circulation $\Gamma(\gamma)$ generated by the bound vortex. The lifting force L acting on the airfoil is defined as:

$$L = \rho U \Gamma \ldots\ldots\ldots\ldots\ldots\ldots\ldots\ldots\ldots\ldots (1)$$

Where $\Gamma = \oint u.dl$ is proportional to the circulation around the wing.

If the effective angle of attack is α, the length of the wing l, and the chord length of the airfoil is c, with the Joukowski transformation the magnitude of the circulation id found as $\Gamma = \pi\alpha cUl$.

$$\mathbf{L = \pi\alpha\rho clU^2 = \frac{1}{2} C_L\rho SU^2} \quad \text{..... (2)}$$

Where $C_L = 2\pi\alpha$ is called the coefficient of lift, S =cl is the area of the airfoil as viewed from an overhead perspective.

The other aerodynamic force that affects an airfoil and is perpendicular to the lifting force, is called drag. This force opposes the relative motion of the airfoil and has direction parallels to the airflow because skin friction drag appear between the air molecules and the surface of the airfoil.

Similarly, the expression for the calculating the drag of airfoil is defined as follows:

$$D = \frac{1}{2} C_D\rho AU^2 \quad \text{..... (3)}$$

Where D is the drag force, A is a reference area and $C_D$ is the drag coefficient.

In summery, aerodynamics forces of the airfoil depend on the shape of the airfoil the density viscosity and compressibility of the air and the wing surface area and angle of attack.

Lift co efficient and drag coefficient are two dimensionless coefficient that the aerodynamic forces. From Eq. 2 and Eq 3, these coefficients are determined by the moving body, density and velocity of the airstream and the corresponding reference area.

$$C_L = \frac{2L}{\rho sU^2} = \frac{L}{qS}$$

$$C_D = \frac{2D}{\rho AU^2} = \frac{D}{qA} \quad \text{.....(4)}$$

Where $q = \frac{1}{2} \rho U^2$ is the airstream dynamic pressure. Actually, these coefficients can be approximated using the aerodynamic theory as above, numerically calculated or measured in the wind tunnel of a complete aircraft wing configuration.

## 6.2 Flow Equations

In order to obtain values of lift, drag and moment coefficients as well as the surface pressure distribution, which are needed to evaluate the objective functions, it is necessary to compute the flow or in other words determine the solution of the airflow over the surfaces. From fluid mechanics, there are fundamental equations that govern the behavior of any fluid that flows over a submerged surface. These are the governing equations that derived using the three-fundamental physical principles that central to the macroscopic observations of nature, which are:

- Conservation of mass, i.e. mass can neither be created nor be destroyed.
- Newton's $2^{nd}$ law, i.e. forces is directly proportional to the rate of change of momentum.
- Conservation of energy, i.e. energy can only change from one to another.

These principles have led to the formulation of complex differential equations that essentially describe the governing of fluid motion. These equations are:

- Continuity and Momentum Equations which are known as the Mass conservation equations and the momentum Conservation equation respectively.
- Energy Conservation equation to model the compressibility effects.

These equations must be solved in order to obtain the solution of the flow which is basically the lift, drag, moment, pressure distribution etc. In addition to these fundamental equations, certain transport equations must be solved to model the turbulence which is an important characteristic associated with high Reynolds number flows. The details and derivations of the fundamental and the additional transport equations can be found in various literature. Here only the equations are listed along with a brief explanation.

## 6.3 Turbulence Model

Most flows encountered in engineering practice are turbulent and therefore require different treatment. Turbulent flows are characterized by the following properties:

- Turbulent flows are highly unsteady.
- They are three- dimensional.
- They contain a great deal of vorticity.
- Turbulence increases the rate at which the conserved quantities are stirred.
- This brings fluids of different momentum content into contact.
- Turbulent flows fluctuate on a broad range of length and times scales.

## 6.4 Standard k-ε model

K-epsilon (k-ε) turbulence model is the most common model used in Computational Fluid Dynamics (CFD) to simulate mean flow characteristics for turbulent flow conditions. It is a two equation model which gives a general description of turbulence by means of two transport equations (PDEs). The original impetus for the K-epsilon model was to improve the mixing-length model, as well as to find an alternative to algebraically prescribing turbulent length scales in moderate to high complexity flows.

- The first transported variable is the turbulence kinetic energy (k).
- The second transported variable is the rate of dissipation of turbulence energy (ε).

Unlike earlier turbulence models, k-ε model focuses on the mechanisms that affect the turbulent kinetic energy. The mixing length model lacks this kind of generality.[2] The underlying assumption of this model is that the turbulent viscosity is isotropic, in other words, the ratio between Reynolds stress and mean rate of deformations is the same in all directions.

The exact k-ε equations contain many unknown and unmeasurable terms. For a much more practical approach, the standard k-ε turbulence model (Launder and Spalding, 1974[3]) is used which is based on our best understanding of the relevant processes, thus minimizing unknowns and presenting a set of equations which can be applied to a large number of turbulent applications.

For turbulent kinetic energy k

$$\frac{\partial(\rho k)}{\partial t}+\frac{\partial(\rho k u_i)}{\partial x_i}=\frac{\partial}{\partial x_j}\left[\frac{\mu_t}{\sigma_k}\frac{\partial k}{\partial x_j}\right]+2\mu_t E_{ij}E_{ij}-\rho\epsilon$$

For dissipation ∈

$$\frac{\partial(\rho\epsilon)}{\partial t}+\frac{\partial(\rho\epsilon u_i)}{\partial x_i}=\frac{\partial}{\partial x_j}\left[\frac{\mu_t}{\sigma_\epsilon}\frac{\partial\epsilon}{\partial x_j}\right]+C_{1\epsilon}\frac{\epsilon}{k}2\mu_t E_{ij}E_{ij}-C_{2\epsilon}\rho\frac{\epsilon^2}{k}$$

The equations contain five adjustable constants: $C_\mu$, $\sigma_k$, $\sigma\varepsilon$, $C_1\varepsilon$ , $C_2\varepsilon$. Based on extensive examination of a wide range of turbulent flows, the constant parameters used in the equations take the following values,

$C_\mu = .009$; $\sigma_k = 1.00$; $\sigma\varepsilon = 1.30$; $C_1\varepsilon = 1.44$; $C_2\varepsilon = 1.92$

However, the model encounters some difficulties in:

- Fails to resolve flows with large strains such as swirling flows and curved boundary layers flow.
- Poor performance in rotating flows.

# Chapter 7

## 3D CAD Design & Construction

### 7.1 Design

Solid works was used to design the wings, base mount and the fuselage (for later purpose). The primary scale is 172.5:1 which roughly translates to a length of 157 mm from actual length of a single wing – 27115 mm. The airfoil cross section remains same for all the wings (stock Boeing 787 airfoil).

Figure 24: Airfoil cross section of Boeing 787-800.

All the wings are modified in such way so that it can be slotted in the base mount and fuselage. The base mount is designed in such way that fits and can be fixed to the mount rod of the wind tunnel. The designs are shown below. All the images were renders of 3D CAD designed wings.

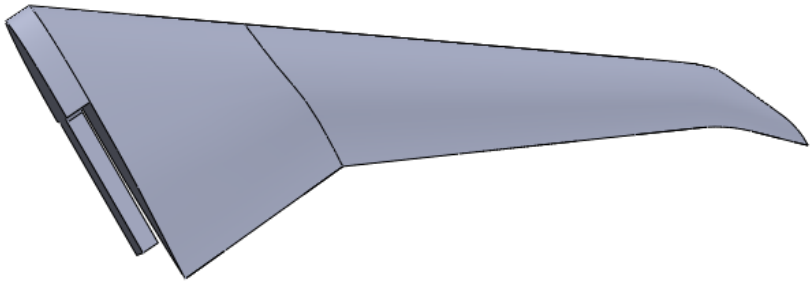

Figure 25: Boeing 787-800 wing with slot.

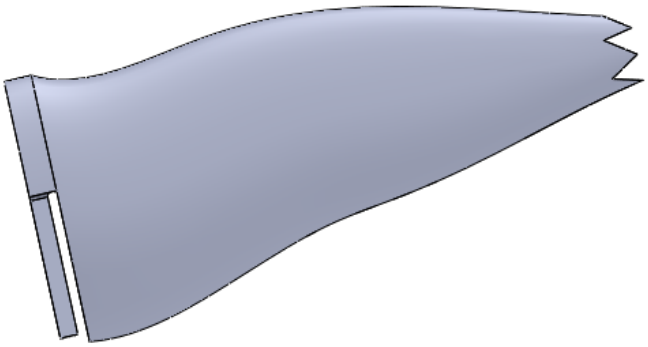

Figure 26: Falcon wing with slot.

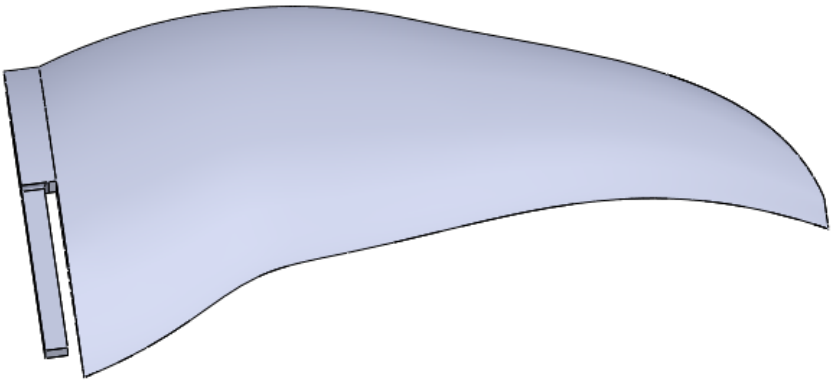

Figure 27: Swift wing with slot

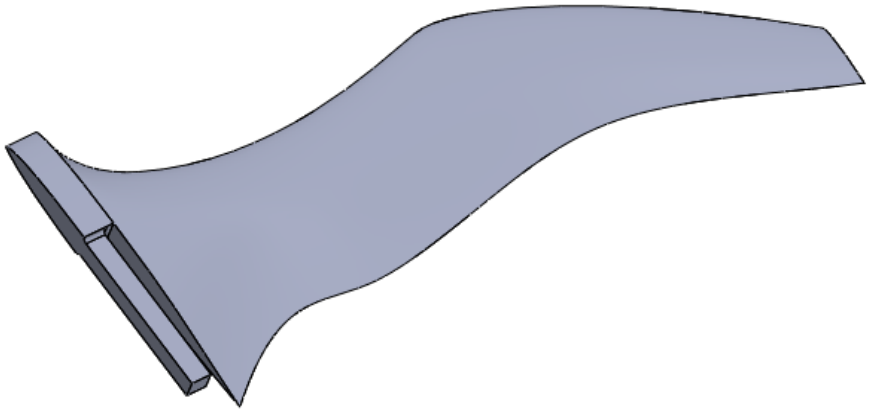

Figure 28: Wandering Albatross wing with slot.

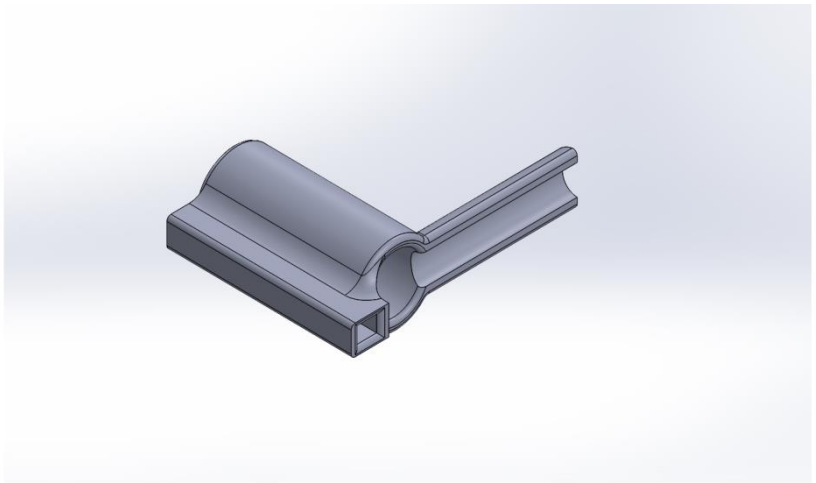

Figure 29: Base mount for single wings and fuselage.

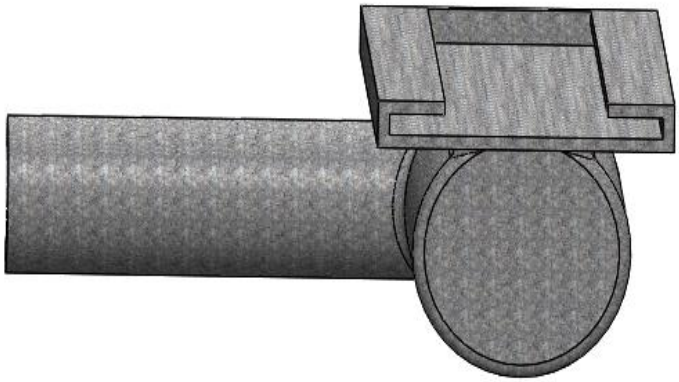

Figure 30: Base mount for full body.

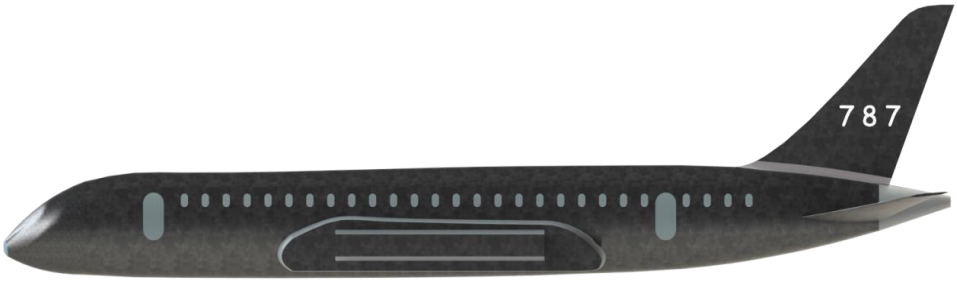


Figure 31: Specially modified fuselage (Boeing 787-800), side view.

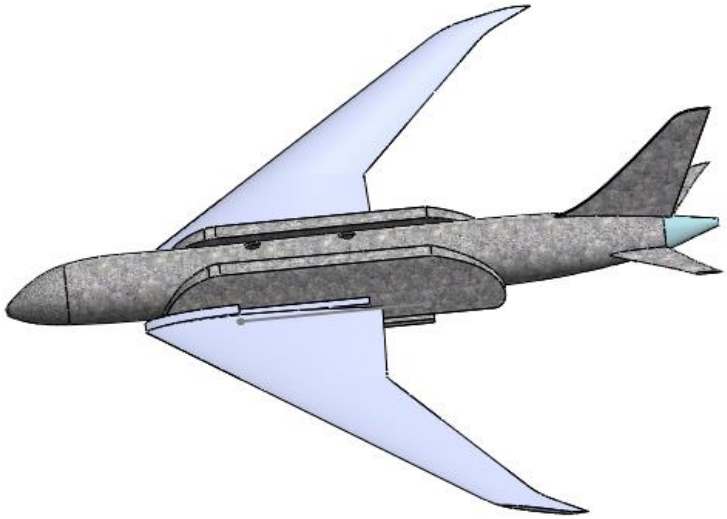

Figure 32: Specially modified fuselage (Boeing 787-800), isometric view.

## 7.2 Construction

The parts were fabricated using 3D printer. Choice of material is ABS plastic which ensured maximum stress resistance while keeping the cost down.

Figure 33: 3D printed Boeing 787-800 single wing(Left).

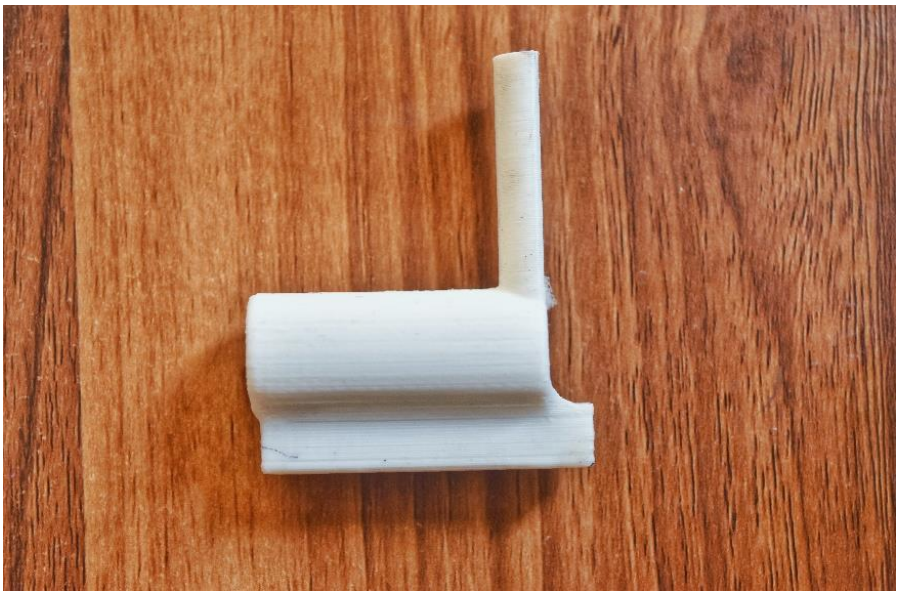

Figure 34: 3D printed base mount.

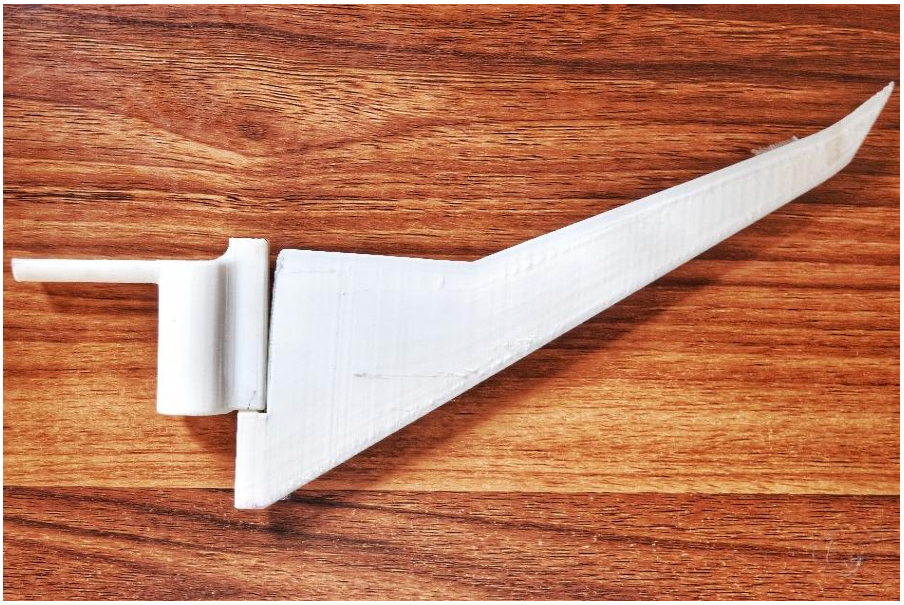

Figure 35: 3D printed Boeing 787-800 single wing with Base mount.

Figure 36: 3D printed Swift wing with Base mount.

Figure 37: 3D printed Falcon wing with Base mount.

Figure 38: 3D printed Wandering Albatross wing with Base mount.

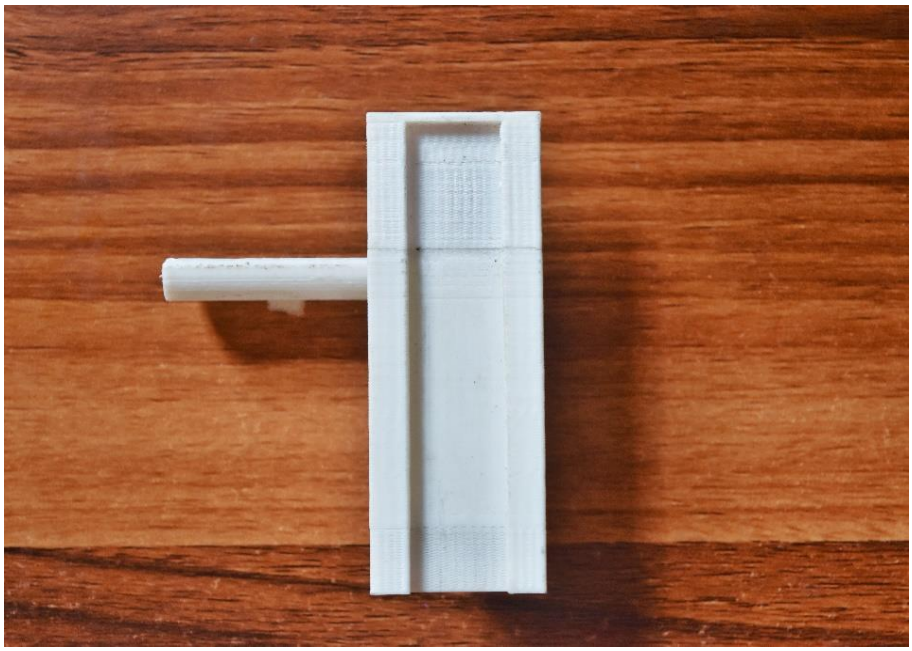

Figure 39: 3D printed Mount for full body

Figure 40: 3D printed Boeing 787-800 fuselage (172.5:6).

Figure 41: 3D printed Boeing 787-800 (172:1).

# Chapter8

## Experimental Setup

### 8.1 Wind Tunnel

A wind tunnel is a tool used in aerodynamic research to study the effects of air moving past solid objects. A wind tunnel consists of a tubular passage with the object under test mounted in the middle.

### Types of Wind Tunnel

Wind Tunnel can be classified on the basis of construction as

a) Open Loop
b) Closed Loop

### a. Open Loop

In an open loop wind tunnel, there is an intake and an exhaust. There is no use for corners and long diffusers but the power needed to drive the wind-tunnel is high because of the loss of energy in the out- flowing air. The open circuit wind tunnel is the simplest and most affordable to build. In these tunnels air is expelled directly into the laboratory and typically reinvested after circulating through the lab, though some tunnels utilize instead a compressed gas source. In addition to their low costs, open circuit tunnels are also advantageous because they have been relatively immune to temperature fluctuations and large disturbances in return flow, provided that the volume of the laboratory is much greater than that of the tunnel.

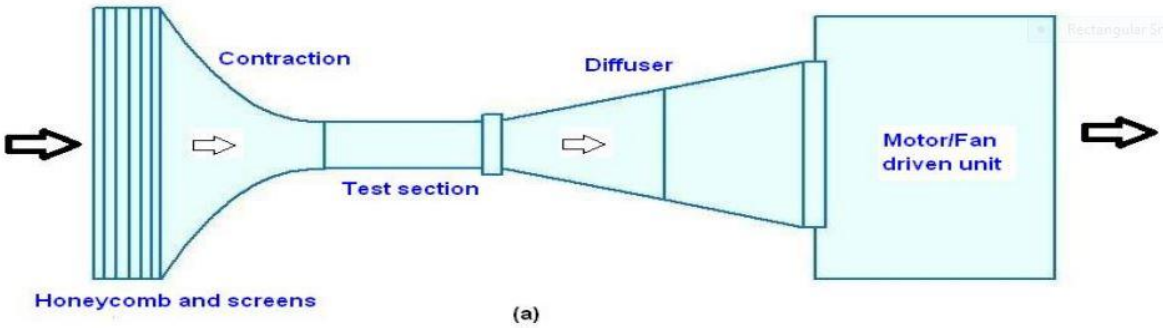


Figure 42: Open Loop Wind Tunnel.

## b. Closed Loop

As the name implies, closed circuit tunnels (also called closed return) form an enclosed loop in which exhaust flow is directly returned to the tunnel inlet. In a closed loop wind tunnel, the air is recalculated to improve efficiency for high speed testing. These tunnels are usually larger and more difficult to build. They must be carefully designed in order to maximize uniformity in the return flow. These tunnels are powered by axial fan(s) upstream of the test section and sometime include multistage compressors, which are often necessary to create trans-sonic and supersonic air speeds. Closed circuit wind-tunnels recirculation the air and thus normally need less power to achieve a given low speed, and, above all, facilitate the achievement of well controlled low conditions in the test section. The present, and most low-speed tunnels used for research, are of the closed-circuit type.

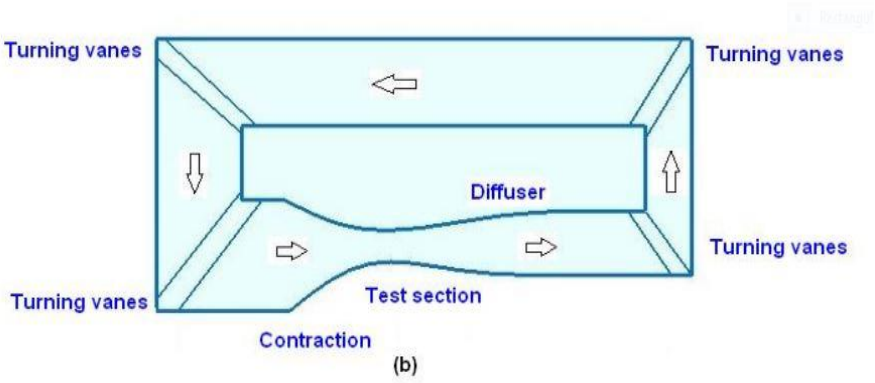


Figure43: Closed Loop Wind Tunnel.

There are many different kinds of wind tunnels

- Low speed wind tunnel
- High speed wind tunnel
- Subsonic & transonic wind tunnel
- Supersonic wind tunnel
- Hypersonic wind tunnel

For our experiment we used subsonic open loop wind tunnel & it's specification is

| **Model** | **AF100 Subsonic Wind Tunnel** |
|---|---|
| **Mass** | 41 kg |
| **Supply** | 3PH |
| **Volts** | 380-440V |
| **Frequency** | 50Hz |
| **Current** | 16A |

Table: Wind Tunnel Specification.

## 8.2 Work Principle

When the sensor driven by a driver is making a linear uniform motion along the test surface, the contact stylus being perpendicular to the work surface, moves up and down with the work surface. Its motion is converted into electric signals, which are amplified, filtered and transformed into digital signals through a/d. the signals are then processed by the CPU into Ra and Rz values before being displayed on the screen.

## 8.3 Experimental Procedure

Figure 44: Subsonic Wind Tunnel

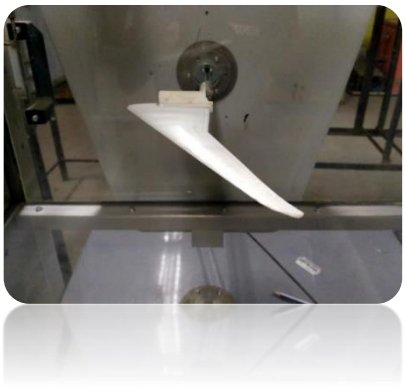

Figure 45: Measuring drag force

Figure 46: Testing Section with full body

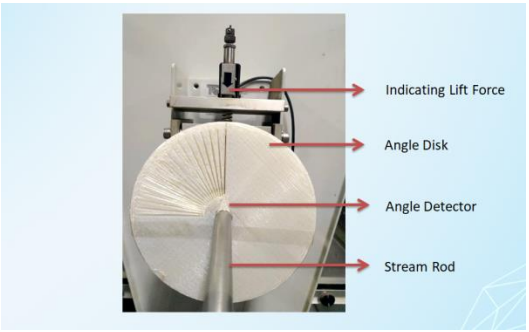


Figure 47: Angle Measuring Disk

# Chapter 9

## METHODOLOGY

- Pitot tube was used to equalize the pressure difference at inlet and outlet section.
- Data was recorded through wind tunnel.

To record the value for the five different cases same procedure was followed.

- Case-1: Mount with different angle (for Drag & Lift force measurement).
- Case-2: Boeing 787-800 wing at different angle of attack (for Drag & Lift force measurement)
- Case-3: Swift (Bird wing) at different angle of attack (for Drag & Lift force measurement)
- Case-3: Albatross (Bird wing) at different angle of attack (for Drag & Lift force measurement)
- Case-4: : Falcon (Bird wing) at different angle of attack (for Drag & Lift force measurement)

## 9.1 Similitude

To find solutions to numerous complicated problems in hydraulic engineering and fluid mechanics, model studies are usually conducted. In order that results obtained in the model studies represent the behavior of prototype, the following similarities must be ensured between the model and the prototype.

## 9.1 Geometric Similarity

For geometric similarity to exist between the model and prototype the ratios of corresponding lengths in the model and in the prototype must be same and the included angles between two corresponding sides must be the same. Models which are not geometrically similar are known as geometrically distorted models.

Let,

$L_m$ = Length of the model

$L_p$ = Length of the prototype

$W_m$ = Width of the model

$W_p$ = Width of the prototype

$H_m$ = Height of the model

$H_p$ = Height of the prototype

Now,

$L_m/L_p$ = 27100/157=172.5

$W_m/W_p$ =12156/70.43=172.5

$H_m/H_p$ = 1019.5/5.91=172.5

So, $L_m/L_p = W_m/W_p = H_m/H_p$; that means, the prototype of the aircraft is geometrically similar as model.

## 9.2 Flow Similarity

We have emphasized two parameters, $R_e$ and $M_s$. For many aerodynamic applications; these are by far the dominant similarity parameters. Therefore, in a limited sense, but applicable to many problems, we can say that flows over geometrically similar bodies at the same Mach and Reynolds number are dynamically similar, and hence the drag will be identical for the bodies.

$(M_a)_m / (M_a)_p = (V/C)_m \times (C/V)_p$

$= (12.86 / 331) \times (331 / 12.86)$

$= 1$

# Chapter 10

## NUMERICAL SOLUTION

### 10.1 Geometry

A three-dimensional wing was taken which surface is smooth. The diameter of wing is 10mm as shown in Figure 22. The model was developed in Solid works 16 then it is imported in ANSYS.

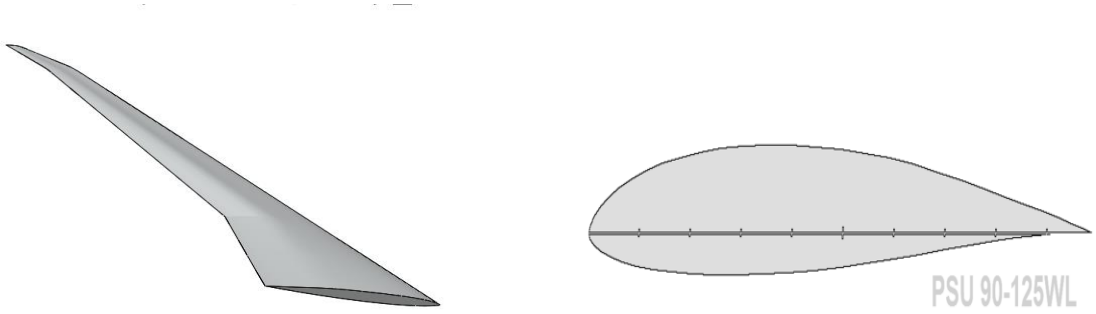


Figure 48: Boeing 787-800 wing and cross section of airfoil.

### 10.2 Computational Domain

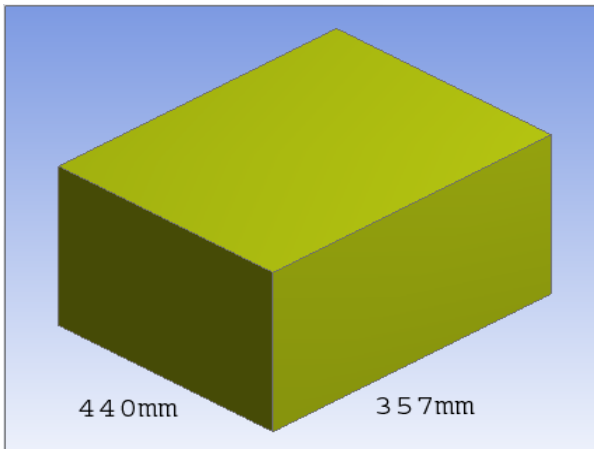


Figure 49: Computational domain for wing.

The numerical study was performed using ANSYS FLUENT. The geometry mounted horizontally in the middle where the all four ends are fixed. The origin of the cartesian system is located at the center wing. The complete setup shown in Figure 49.

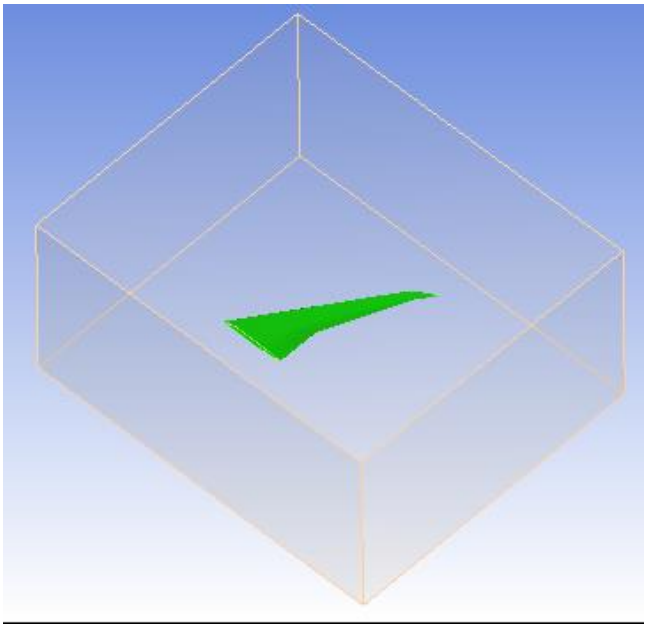

Figure 50: Wing located in the center of the 3D domain in ANSYS.

## 10.3 Meshing

**Me**shing was done using doing ANSYS MESH software. Curvature is used as Advanced Size Function. From boundary wall coarse mesh is done and fine mesh is done near the wing. Figure 50 shows the mesh around wing.

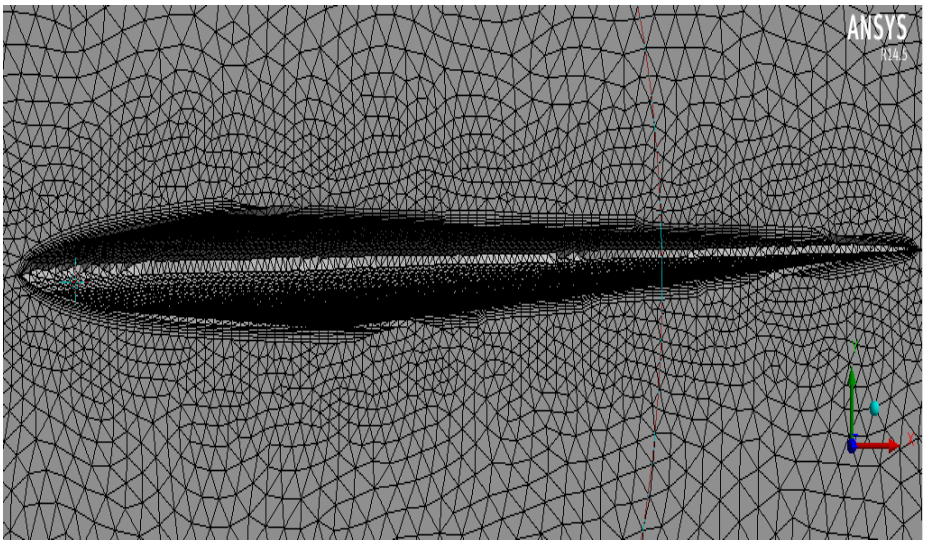


Figure 51: Mesh around the wing.

## 10.4 Setup

k-$\omega$ standard model is used for solution. The standard k-$\omega$ model is very similar in structure to the k-$\omega$ model but the variables replaced by the dissipation rate per unit kinetic energy, $\omega$. The advantage of the standard k-$\omega$ model comapared to the standard k-$\omega$ is that the $\omega$ equation is more robust and easier to integrate compared to the equation the need of additional damping functions.

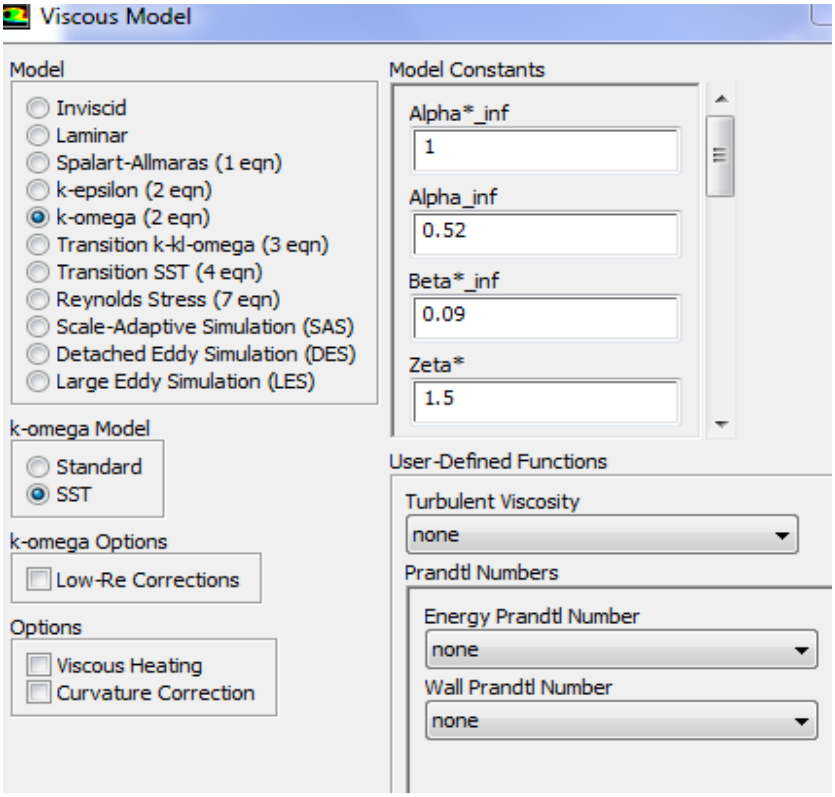


Figure 52: Setup chart in ANSYS 17

## 10.5 Boundary Conditions

The boundary conditions are given in the table

| Boundary condition | |
|---|---|
| **X- Velocity** | 12.86 m/s |
| **Y- Velocity** | 0 |
| **Z- Velocity** | 0 |
| **Turbulent Intensity** | 5% |
| **Turbulent Viscosity Ratio** | 10 |
| **Gauge Pressure** | 0 Pascal |
| **Turbulent Intensity** | 5% |
| **Turbulent Viscosity Ratio** | 10 |
| **Wall motion** | Stationary wall |
| **Shear condition** | No slip |
| **Wall motion** | Stationary wall |
| **Shear condition** | No slip |

Solution method scheme Simple is used. For gradient, pressure, momentum, turbulent kinetic energy and specific dissipation rate following methods are used least squares cell based, second order upwind and first order upwind respectively.

## 10.6 Airfoil

For airfoil designing the Air liner (NACA 2415) cross section has been selected, Which is commercially used for passenger airliner i.e, Boeing 787-800.

Figure 53: NACA 2451 airfoil cross section.

## 10.7 Wing Specification

Wing length: 157 mm

Airfoil diameter: 10 mm

Airfoil cross section width at root = 60 mm

# Chapter 11

## Result & Calculation

In this experiment the fabrication of wings is done as per design made. The main motive of the experiment was to compare the drag and lift of different geometry shape wings.

The graphs that are achieved from experimental data are-

- Drag Vs. Velocity
- Lift Vs. Velocity
- Drag Vs. Angle of attack
- Lift Vs. Angle of attack

## 11.1 Drag VS. Velocity for Wandering Albatross

The graph shows that the value for different angle of with the increment of velocity the drag force also increases

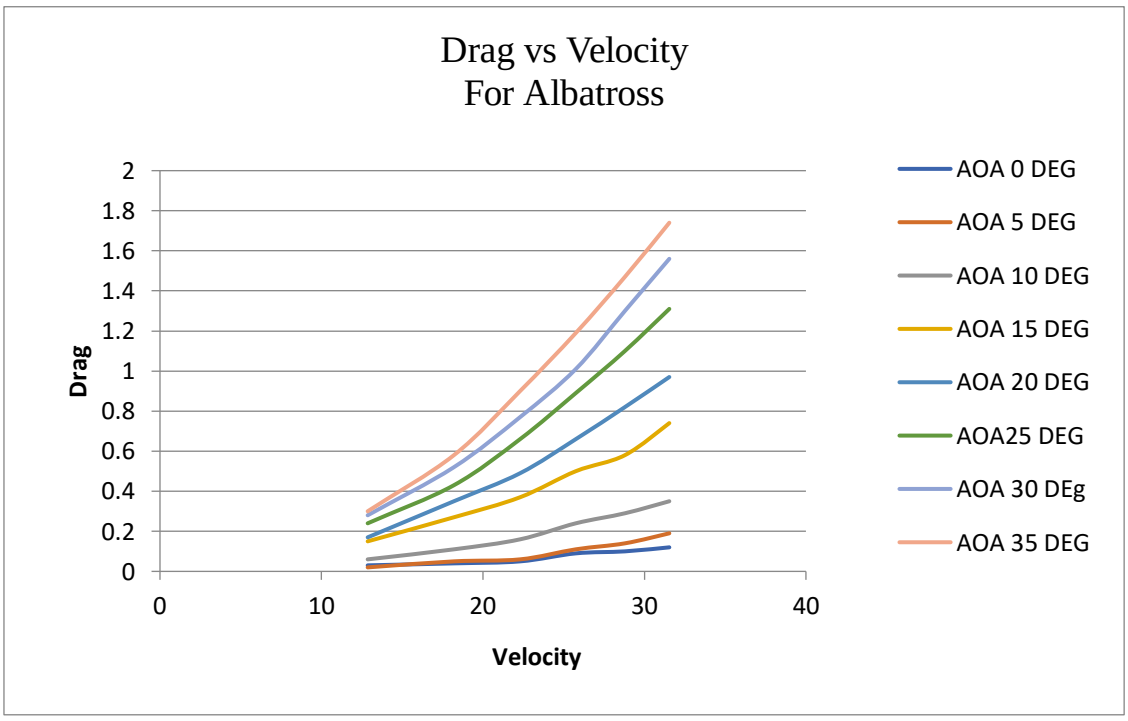

## 11.2 Lift Vs. Velocity for Boeing 787-800

The lift also increases with velocity but for a stall velocity the lift starts to fall down which may not be shown in the graph as the velocity had a limit for the wind tunnel it is experimented.

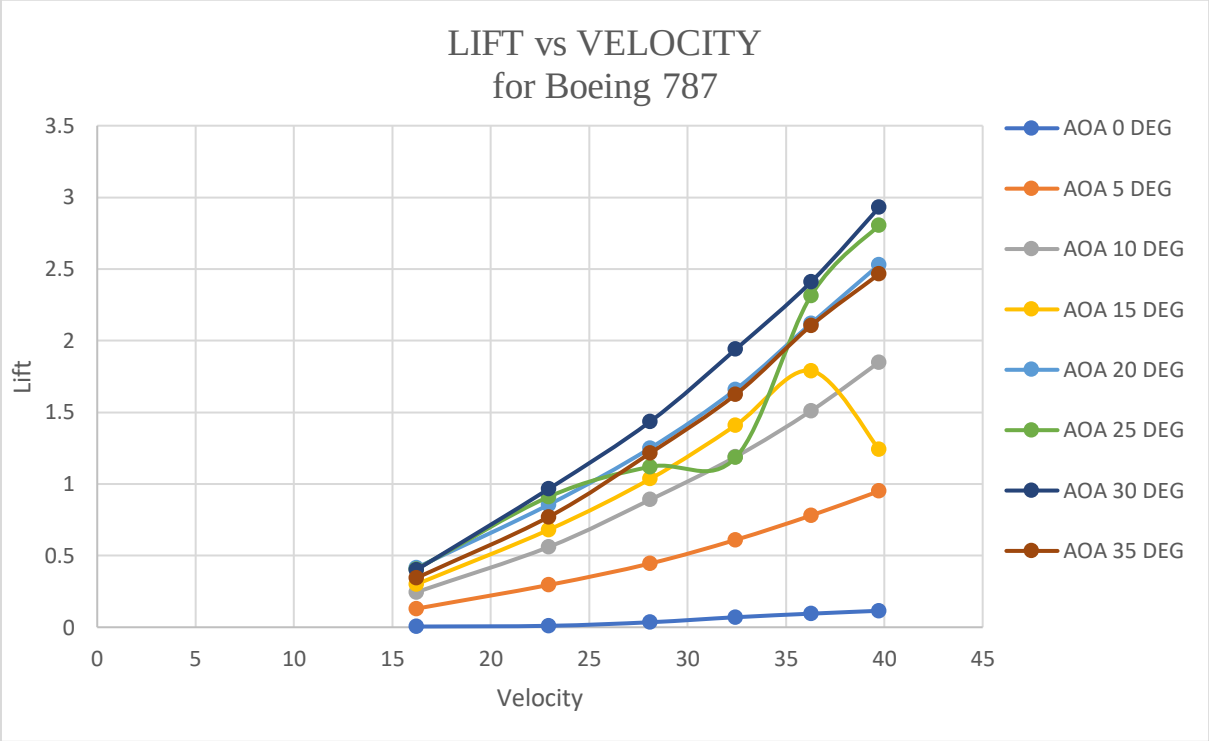


## 11.3 Lift Vs. Angle of attack

This graph shows the increment of lift up to a critical angle of attack. The swift has the quick increment in lift the albatross has less lift compared to others among this graphs Boeing 787-800 has the better lift generation.

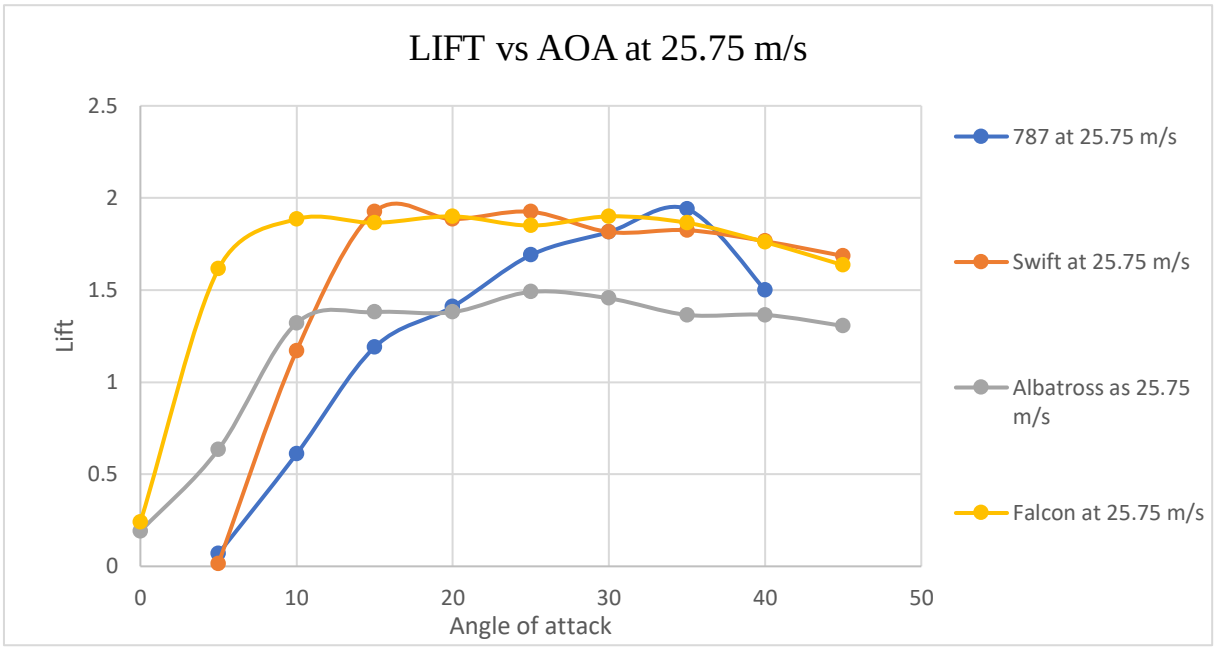


## 11.4 Drag Vs. Angle of attack

This graph shows increase in drag with angle of attack. The drag generation is less than the lift which plays a vital role in take-off of an airplane.

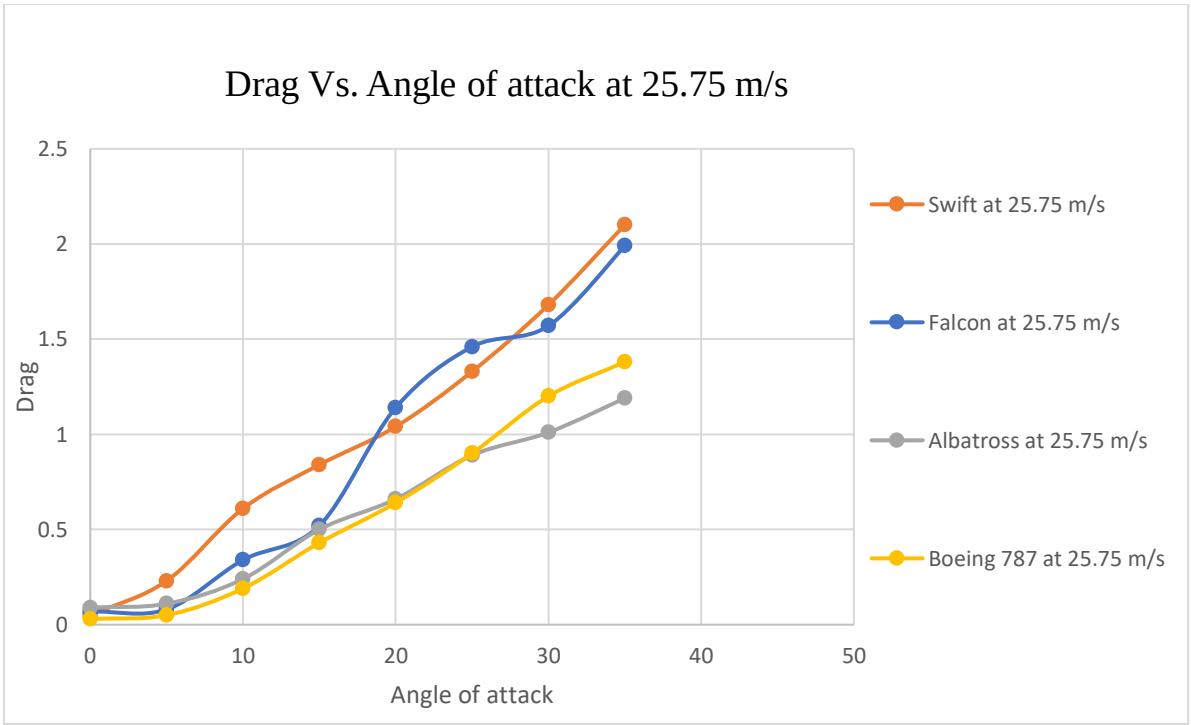

## 11.5 Calculation

- **Dimension of prototype & Model**

Wingspan of prototype, $L_p$= 60,000 mm

Fuselage Width of prototype, $W_p$ = 5770 mm

Single wing length of prototype, $l_p$ = 27,100 mm

Considered Ratio = 172.5

Now,

Single wing length of model, $l_m$ = 228.5 mm

- **Projected area of wing**

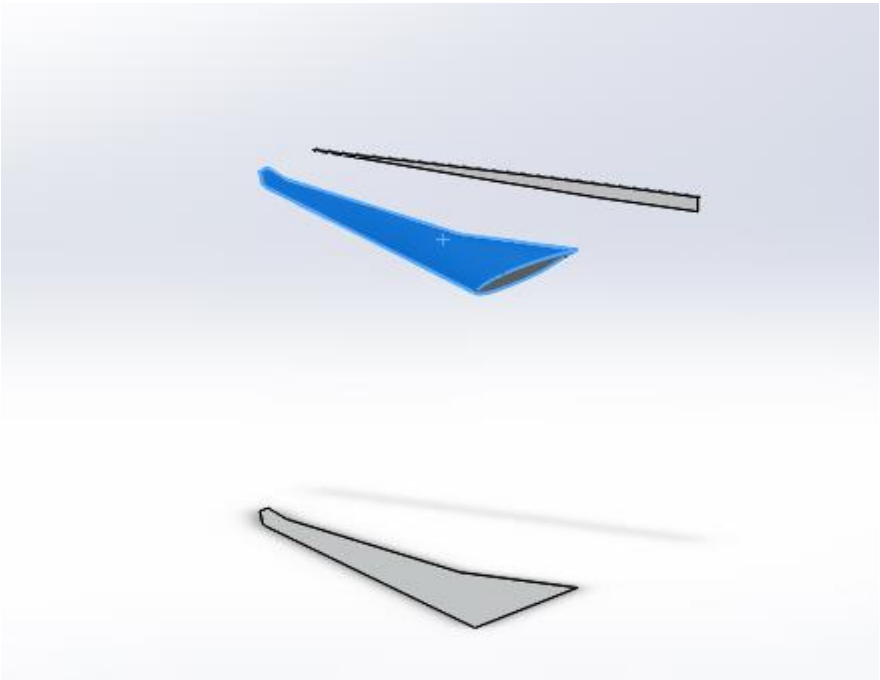

Figure 52: Projected area reflected on a plane.

Projected area for Drag force = 603.4 $mm^2$

Projected area for Lift force =5 333.62 $mm^2$

(I.e. Projected areas are calculated using solid works)

## Hydraulic diameter

$$\text{Hydraulic Diameter, } D_H = \frac{4 \times \text{Area}}{2 \times \text{Wetted Perimeter}}$$

$$= \frac{4 \times (.305 \times .305)}{2 \times (.305 + .305)}$$

$$= 0.305$$

Where,

Height, H = 0.305 m

Width, W = 0.305 m

Area = H × W

Wetted Perimeter =W+H

- When ΔH =10 mm

$H_{air} = \frac{H(water) \times \rho(water)}{\rho air}$ m

$= \frac{0.01 \times 1000}{1.184}$ m

= 8.45 m

where, $H_{ccl4}$ = 10 mm

=0.01 m

$\rho_{water}$ = 1000 kg/m³

$\rho_{air}$ = 1.184 kg/m³

$V = \sqrt{2 \times g \times Hair}$

$= \sqrt{2 \times 9.81 \times 8.45}$

= 12.86 m/s

Now,

We know,

$$C_d = \frac{\text{Drag force}}{\frac{1}{2} \times \rho air \times V^2 \times A}$$

$$C_d = \frac{\text{Drag force}}{\frac{1}{2} \times \rho air \times V^2 \times A}$$

$$= \frac{.05}{\frac{1}{2} \times 1.184 \times 12.86^2 \times 0.000847}$$

$$= 0.60$$

Again,

$$C_l = \frac{\text{Lift force}}{\frac{1}{2} \times \rho air \times V^2 \times A}$$

$$C_l = \frac{.24}{\frac{1}{2} \times 1.184 \times 12.86 \times .005237}$$

$$=0.45$$

Here,

Drag force = 0.05 N

$\rho_{air}$ = 1.184 kg/m³

Velocity=12.86 m/s

Projected area,

Drag P.A = 0.000847 m²

Lift P.A = 0.005237 m²

# Chapter 12

## Cost Analysis

| Items | Cost |
|---|---|
| Wings<br>➢ Albatross<br>➢ Falcon<br>➢ Swift<br>➢ 787 | 770/-<br>1040/-<br>890/-<br>760/- |
| Mount<br>➢ For full body<br>➢ For wings | 442/-<br>760/- |
| Tub for 5 different angle | 2625/- |
| Full body | 1948/- |
| Extra | 1000/- |
| Wastage | 2000/- |
| Total | 12235/- |

The above expenses are for present thesis condition. As we know our thesis materials are made by 3D printer which is currently not so much easily available in Bangladesh and their demand is so much high that's why our wastage amount is like this figure. We used Plastics (PL) which cost 23 taka per centimeter cube. We choose Plastic for better surface finishing and strong support.

# Chapter 13

## Reference:

» Nature Inspired Inventions and Engineering for Aviation - Outdoor Economy. (n.d.). Retrieved May 3, 2018, from http://outdooreconomy.com/nature-inspired-inventions-and-engineering-for-aviation/

Airbus aircraft design inspired by Nature | Biomimetic Summit Barcelona 2016. (n.d.). Retrieved May 3, 2018, from http://www.biomimeticsummit.com/airbus-aircraft-design-inspired-by-nature/

Aldheeb, M. A., Asrar, W., Sulaeman, E., Omar, A. A., Aldheeb, M. A., Asrar, W., … Omar, A. A. (2016). A Review on Aerodynamics of Non-Flapping Bird Wings. *Journal of Aerospace Technology and Management*, *8*(1), 7–17. https://doi.org/10.5028/jatm.v8i1.564

Angle of Attack for Airfoil. (n.d.). Retrieved May 3, 2018, from http://hyperphysics.phy-astr.gsu.edu/hbase/Fluids/angatt.html

ARNOLD, E. N. (2002). Holaspis, a lizard that glided by accident: mosaics of cooption and adaptation in a tropical forest lacertid (Reptilia, Lacertidae). *Bulletin of The Natural History Museum. Zoology Series*, *68*(02), 155–163. https://doi.org/10.1017/S0968047002000171

Bernoulli's Equation. (n.d.). Retrieved May 3, 2018, from https://www.grc.nasa.gov/www/k-12/airplane/bern.html

Berra, T. M., & Berra, T. M. (2001). *Freshwater fish distribution*. Academic Press.

Corlett, R., & Primack, R. B. (2011). *Tropical rain forests : an ecological and biogeographical comparison* (2nd ed.). Chichester: Wiley-Blackwell. Retrieved from https://books.google.com/books?id=R0j8NROHQi8C&pg=PA197&lpg=PA197&dq=south+american+gliding+frog&source=bl&ots=sRvEGT5a8F&sig=cLFndvIrNFzOzlBTzPuGh93AQg0&hl=en&sa=X&ei=PFRJT-86gefRAf_SrKUO&ved=0CEYQ6AEwBQ#v=onepage&q=south american gliding frog&f=false

Cronin, L. (1991). *Key guide to Australian mammals*. Reed Books.

Dzik, J., & Sulej, T. (2016). An early Late Triassic long-necked reptile with a bony pectoral shield and gracile appendages. *Acta Palaeontologica Polonica*, *64*(4), 805–823. Retrieved from https://www.app.pan.pl/archive/published/app61/app002762016.pdf

Emerson, S. B., & Koehl, M. A. R. (1990). The Interaction of Behavioral and Morphological Change in the Evolution of a Novel Locomotor Type: "Flying" Frogs. *Evolution*, *44*(8), 1931. https://doi.org/10.2307/2409604

Gaetano, L. C., & Rougier, G. W. (2011). New materials of *Argentoconodon fariasorum* (Mammaliaformes, Triconodontidae) from the Jurassic of Argentina and its bearing on triconodont phylogeny. *Journal of Vertebrate Paleontology*, *31*(4), 829–843. https://doi.org/10.1080/02724634.2011.589877

How animals inspire aircraft design | PrivateFly Blog. (n.d.). Retrieved May 3, 2018, from https://blog.privatefly.com/how-animals-inspire-aircraft-design

Jenett, B., Calisch, S., Cellucci, D., Cramer, N., Gershenfeld, N., Swei, S., & Cheung, K. C. (2017). Digital Morphing Wing: Active Wing Shaping Concept Using Composite Lattice-Based Cellular Structures. *Soft Robotics*, *4*(1), 33–48. https://doi.org/10.1089/soro.2016.0032

Kaplan, M. (2011). Ancient bats got in a flap over food. *Nature*. https://doi.org/10.1038/nature.2011.9304

*Life in the Rainforest*. (n.d.). Retrieved from http://www.szgdocent.org/resource/ff/f-rain1a.htm

Macia, S., Robinson, M. P., Craze, P., Dalton, R., & Thomas, J. D. (2004). New observations on airborne jet propulsion (flight) in squid, with a review of previous reports. *Journal Molluscan Studies*, *70*(3), 297–299. https://doi.org/10.1093/mollus/70.3.297

McCracken, G. F., Safi, K., Kunz, T. H., Dechmann, D. K. N., Swartz, S. M., & Wikelski, M. (2016). Airplane tracking documents the fastest flight speeds recorded for bats. *Royal Society Open Science*, *3*(11), 160398. https://doi.org/10.1098/rsos.160398

McGuire, J. A. (2003). Allometric prediction of locomotor performance: an example from

Southeast Asian flying lizards. *The American Naturalist*, *161*(2), 337–339. https://doi.org/10.1086/346085

Mendelson, J. R., Savage, J. M., Griffith, E., Ross, H., Kubicki, B., & Gagliardo, R. (2008). Spectacular New Gliding Species of Ecnomiohyla (Anura: Hylidae) from Central Panama. *Journal of Herpetology*, *42*(4), 750. https://doi.org/10.1670/08-025R1.1

Meng, Q.-J., Grossnickle, D. M., Liu, D., Zhang, Y.-G., Neander, A. I., Ji, Q., & Luo, Z.-X. (2017). New gliding mammaliaforms from the Jurassic. *Nature*, *548*(7667), 291–296. https://doi.org/10.1038/nature23476

Muijres, F. T., Christoffer Johansson, L., Bowlin, M. S., Winter, Y., Hedenströ, A., & Humphries, S. (2012). Comparing Aerodynamic Efficiency in Birds and Bats Suggests Better Flight Performance in Birds. https://doi.org/10.1371/journal.pone.0037335

Myers, P. (n.d.). *Family Pseudocheiridae*. Retrieved from http://animaldiversity.ummz.umich.edu/site/accounts/information/Pseudocheiridae.html

Newtonian Principle. (n.d.). Retrieved May 3, 2018, from http://ffden-2.phys.uaf.edu/webproj/211_fall_2014/Thor_Austin/thor_austin/Newtonian Principle.html

PACKARD, A. (1972). CEPHALOPODS AND FISH: THE LIMITS OF CONVERGENCE. *Biological Reviews*, *47*(2), 241–307. https://doi.org/10.1111/j.1469-185X.1972.tb00975.x

Photopoulos, J. (2016). Speedy bat flies at 160km/h, smashing bird speed record. *New Scientist*. Retrieved from https://www.newscientist.com/article/2112044-speedy-bat-flies-at-160kmh-smashing-bird-speed-record/

Pressure. (n.d.). Retrieved May 3, 2018, from http://hyperphysics.phy-astr.gsu.edu/hbase/Fluids/downwash.html

Ride, W. D. L., & Fry, E. (1970). *A guide to the native mammals of Australia*. Oxford University Press.

Russell, R. (1980). *Spotlight on possums*. University of Queensland Press.

Saidel, W. M., Strain, G. F., & Fornari, S. K. (2004). Characterization of the Aerial Escape Response of the African Butterfly Fish, Pantodon buchholzi Peters. *Environmental Biology of Fishes*, *71*(1), 63–72. https://doi.org/10.1023/B:EBFI.0000043153.38418.cd

Sane, S. P. (2003). The aerodynamics of insect flight. *The Journal of Experimental Biology*, *206*(Pt 23), 4191–4208. https://doi.org/10.1242/jeb.00663

Schiotz, A., & Volsoe, H. (1959). The Gliding Flight of Holaspis guentheri Gray, a West-African Lacertid. *Copeia*, *1959*(3), 259. https://doi.org/10.2307/1440407

Scientist Discovers Rainforest Ants That Glide. (n.d.). *Newswise*. Retrieved from http://www.mongabay.com/external/2005/02_09-newswise.html

Serventy, V. (1977). *Wildlife of Australia*. Thomas Nelson (Australia).

Simmons, N. B., & D.E. Wilson, D. C. R. (2005). *Mammal Species of the World: A Taxonomic and Geographic Reference*. Baltimore, MD: Johns Hopkins University Press.

Simmons, N. B., Seymour, K. L., Habersetzer, J., & Gunnell, G. F. (2008). Primitive Early Eocene bat from Wyoming and the evolution of flight and echolocation. *Nature*, *451*(7180), 818–821. https://doi.org/10.1038/nature06549

The 100-Year-Old Idea That Could Change Flight — NOVA Next | PBS. (n.d.). Retrieved May 3, 2018, from http://www.pbs.org/wgbh/nova/next/space/morphing-wings/

Tobalske, B. W., Hearn, J. W. D., & Warrick, D. R. (n.d.). Aerodynamics of intermittent bounds in flying birds. https://doi.org/10.1007/s00348-009-0614-9

Troughton, E., & Cayley, N. W. (1973). *Furred animals of Australia*. Angus & Robertson.

Tudge, C. (2002). *The variety of life : a survey and a celebration of all the creatures that have ever lived*. Oxford University Press.

Vandenbeld, J., & Australian Broadcasting Corporation. (1992). *Nature of Australia : a portrait of the island continent*. Collins Australia.

*Vertebrate Flight: gliding and parachuting*. (n.d.). Retrieved from http://www.ucmp.berkeley.edu/vertebrates/flight/gliding.html

*Vertebrate Flight*. (n.d.). Retrieved from http://www.ucmp.berkeley.edu/vertebrates/flight/enter.html

Wang, S., Zhang, X., He, G., & Liu, T. (2014). Lift enhancement by dynamically changing wingspan in forward flapping flight. *Physics of Fluids*, *26*(6), 061903. https://doi.org/10.1063/1.4884130

Wang, Z. J. (2005). DISSECTING INSECT FLIGHT. *Annual Review of Fluid Mechanics*, *37*(1), 183–210. https://doi.org/10.1146/annurev.fluid.36.050802.121940

What Is Fluid-Structure Interaction? (n.d.). Retrieved May 3, 2018, from https://www.comsol.com/multiphysics/fluid-structure-interaction

Withers, P. C. (1981). AN AERODYNAMIC ANALYSIS OF BIRD WINGS AS FIXED AEROFOILS. *J. Exp. Biol*, *90*, 143–162. Retrieved from https://pdfs.semanticscholar.org/fabb/0e50ba272d4339ef2a9932bdfeca83024d9e.pdf

Xu, X., Zhou, Z., Wang, X., Kuang, X., Zhang, F., & Du, X. (2003). Four-winged dinosaurs from China. *Nature*, *421*(6921), 335–340. https://doi.org/10.1038/nature01342

Yanoviak, S. P., Dudley, R., & Kaspari, M. (2005). Directed aerial descent in canopy ants. *Nature*, *433*(7026), 624–626. https://doi.org/10.1038/nature03254

Yanoviak, S. P., Kaspari, M., & Dudley, R. (2009). Gliding hexapods and the origins of insect aerial behaviour. *Biology Letters*, *5*(4), 510–512. https://doi.org/10.1098/rsbl.2009.0029

# APPENDICES

## Appendix A

**Table A-1: Average experimental Drag & Lift value for Boeing 787-800.**

| Angle of attack (degree) | Velocity (m/s) | Lift(N) | Drag (N) |
|---|---|---|---|
| 0° | 12.86 | .005 | .005 |
| | 18.20 | .01 | .01 |
| | 22.30 | .035 | .02 |
| | 25.75 | .07 | .03 |
| | 28.79 | .095 | .04 |
| | 31.54 | .115 | .04 |
| 5° | 12.86 | .13 | .005 |
| | 18.20 | .295 | .02 |
| | 22.30 | .445 | .03 |
| | 25.75 | .61 | .05 |
| | 28.79 | .78 | .07 |
| | 31.54 | .95 | .12 |

| Angle of attack (degree) | Velocity (m/s) | Lift(N) | Drag (N) |
|---|---|---|---|
| **10°** | 12.86 | .245 | .06 |
| | 18.20 | .56 | .09 |
| | 22.30 | .89 | .14 |
| | 25.75 | 1.19 | .19 |
| | 28.79 | 1.51 | .25 |
| | 31.54 | 1.85 | .27 |
| **15°** | 12.86 | .3 | .09 |
| | 18.20 | .68 | .21 |
| | 22.30 | 1.03 | .31 |
| | 25.75 | 1.41 | .43 |
| | 28.79 | 1.79 | .53 |
| | 31.54 | 2.24 | .72 |

| Angle of attack (degree) | Velocity (m/s) | Lift(N) | Drag (N) |
|---|---|---|---|
| **20°** | 12.86 | .415 | .16 |
| | 18.20 | .855 | .33 |
| | 22.30 | 1.25 | .48 |
| | 25.75 | 1.66 | .64 |
| | 28.79 | 2.12 | .84 |
| | 31.54 | 2.53 | 1.05 |
| **25°** | 12.86 | .405 | .19 |
| | 18.20 | .91 | .42 |
| | 22.30 | 1.42 | .63 |
| | 25.75 | 1.82 | .90 |
| | 28.79 | 2.32 | 1.15 |
| | 31.54 | 2.81 | 1.37 |

| Angle of attack (degree) | Velocity (m/s) | Lift(N) | Drag (N) |
|---|---|---|---|
| **30°** | 12.86 | .4 | .24 |
| | 18.20 | .97 | .57 |
| | 22.30 | 1.44 | .87 |
| | 25.75 | 1.94 | 1.2 |
| | 28.79 | 2.41 | 1.55 |
| | 31.54 | 2.93 | 1.85 |
| **35°** | 12.86 | .25 | .29 |
| | 18.20 | .7 | .63 |
| | 22.30 | 1.15 | 1.05 |
| | 25.75 | 1.5 | 1.38 |
| | 28.79 | 2.05 | 1.77 |
| | 31.54 | 2.47 | 2.12 |

**Table A-2: Average experimental Drag & Lift value for Swift**.

| Angle of attack (degree) | Velocity (m/s) | Lift(N) | Drag (N) |
|---|---|---|---|
| **0°** | 12.86 | .01 | .03 |
| | 18.20 | .015 | .03 |
| | 22.30 | .02 | .03 |
| | 25.75 | .015 | .05 |
| | 28.79 | .025 | .03 |
| | 31.54 | .025 | .06 |
| **5°** | 12.86 | .215 | .05 |
| | 18.20 | .47 | .1 |
| | 22.30 | .775 | .12 |
| | 25.75 | 1.17 | .23 |
| | 28.79 | 1.705 | .33 |
| | 31.54 | 2.3 | .5 |

| Angle of attack (degree) | Velocity (m/s) | Lift(N) | Drag (N) |
|---|---|---|---|
| **10°** | 12.86 | .43 | .14 |
| | 18.20 | .905 | .29 |
| | 22.30 | 1.395 | .44 |
| | 25.75 | 1.925 | .61 |
| | 28.79 | 2.305 | .78 |
| | 31.54 | 2.93 | 1.01 |
| **15°** | 12.86 | .445 | .2 |
| | 18.20 | .97 | .41 |
| | 22.30 | 1.365 | .6 |
| | 25.75 | 1.885 | .84 |
| | 28.79 | 2.35 | 1.09 |
| | 31.54 | 3.01 | 1.44 |

| Angle of attack (degree) | Velocity (m/s) | Lift(N) | Drag (N) |
|---|---|---|---|
| **20°** | 12.86 | .48 | .25 |
| | 18.20 | .96 | .52 |
| | 22.30 | 1.54 | .77 |
| | 25.75 | 1.925 | 1.04 |
| | 28.79 | 2.47 | 1.32 |
| | 31.54 | 2.875 | 1.63 |
| **25°** | 12.86 | .425 | .33 |
| | 18.20 | .945 | .68 |
| | 22.30 | 1.13 | .99 |
| | 25.75 | 1.815 | 1.33 |
| | 28.79 | 2.67 | 1.72 |
| | 31.54 | 2.64 | 2.19 |

| Angle of attack (degree) | Velocity (m/s) | Lift(N) | Drag (N) |
|---|---|---|---|
| **30°** | 12.86 | .46 | .4 |
| | 18.20 | .91 | .83 |
| | 22.30 | 1.38 | 1.23 |
| | 25.75 | 1.83 | 1.68 |
| | 28.79 | 2.30 | 2.17 |
| | 31.54 | 2.77 | 2.7 |
| **35°** | 12.86 | .44 | .53 |
| | 18.20 | .9 | 1 |
| | 22.30 | 1.35 | 1.51 |
| | 25.75 | 1.76 | 2.1 |
| | 28.79 | 2.17 | 2.6 |
| | 31.54 | 2.65 | 3.2 |

**Table A-3: Average experimental Drag & Lift value for Wandering Albatross.**

| Angle of attack (degree) | Velocity (m/s) | Lift(N) | Drag (N) |
|---|---|---|---|
| **0°** | 12.86 | .035 | .03 |
| | 18.20 | .08 | .04 |
| | 22.30 | .14 | .05 |
| | 25.75 | .19 | .09 |
| | 28.79 | .25 | .1 |
| | 31.54 | .3 | .12 |
| **5°** | 12.86 | .09 | .02 |
| | 18.20 | .23 | .05 |
| | 22.30 | .42 | .06 |
| | 25.75 | .64 | .11 |
| | 28.79 | .93 | .14 |
| | 31.54 | 1.17 | .19 |

| Angle of attack (degree) | Velocity (m/s) | Lift(N) | Drag (N) |
|---|---|---|---|
| **10°** | 12.86 | .3 | .06 |
| | 18.20 | .65 | .11 |
| | 22.30 | 1.04 | .16 |
| | 25.75 | 1.32 | .24 |
| | 28.79 | 1.74 | .29 |
| | 31.54 | 2.12 | .35 |
| **15°** | 12.86 | .32 | .15 |
| | 18.20 | .64 | .27 |
| | 22.30 | 1 | .37 |
| | 25.75 | 1.38 | .5 |
| | 28.79 | 1.75 | .58 |
| | 31.54 | 2.01 | .78 |

| Angle of attack (degree) | Velocity (m/s) | Lift(N) | Drag (N) |
|---|---|---|---|
| **20°** | 12.86 | .31 | .17 |
| | 18.20 | .7 | .35 |
| | 22.30 | 1 | .49 |
| | 25.75 | 1.4 | .66 |
| | 28.79 | 1.77 | .83 |
| | 31.54 | 2.14 | .97 |
| **25°** | 12.86 | .39 | .24 |
| | 18.20 | .74 | .43 |
| | 22.30 | 1.00 | .66 |
| | 25.75 | 1.49 | .89 |
| | 28.79 | 1.86 | 1.1 |
| | 31.54 | 2.25 | 1.31 |

| Angle of attack (degree) | Velocity (m/s) | Lift(N) | Drag (N) |
|---|---|---|---|
| **30°** | 12.86 | .37 | .28 |
| | 18.20 | .68 | .52 |
| | 22.30 | .99 | .77 |
| | 25.75 | 1.45 | 1.01 |
| | 28.79 | 1.85 | 1.3 |
| | 31.54 | 2.24 | 1.56 |
| **35°** | 12.86 | .31 | .3 |
| | 18.20 | .7 | .58 |
| | 22.30 | 1.04 | .9 |
| | 25.75 | 1.36 | 1.19 |
| | 28.79 | 1.74 | 1.47 |
| | 31.54 | 2.16 | 1.74 |

| Angle of attack (degree) | Velocity (m/s) | Lift(N) | Drag (N) |
|---|---|---|---|
| **40°** | 12.86 | .37 | N/A |
| | 18.20 | .74 | N/A |
| | 22.30 | 1.03 | N/A |
| | 25.75 | 1 | N/A |
| | 28.79 | 1.70 | N/A |
| | 31.54 | 2 | N/A |
| **45°** | 12.86 | .3 | N/A |
| | 18.20 | .65 | N/A |
| | 22.30 | .98 | N/A |
| | 25.75 | 1.3 | N/A |
| | 28.79 | 1.53 | N/A |
| | 31.54 | 1.88 | N/A |

**Table A-4: Average experimental Drag & Lift value for Falcon.**

| Angle of attack (degree) | Velocity (m/s) | Lift(N) | Drag (N) |
|---|---|---|---|
| **0°** | 12.86 | .03 | .01 |
| | 18.20 | .095 | .04 |
| | 22.30 | .15 | .06 |
| | 25.75 | .24 | .07 |
| | 28.79 | .37 | .08 |
| | 31.54 | .51 | .09 |
| **5°** | 12.86 | .29 | .04 |
| | 18.20 | .65 | .07 |
| | 22.30 | 1.09 | .1 |
| | 25.75 | 1..615 | .08 |
| | 28.79 | 2.23 | .11 |
| | 31.54 | 2.9 | .2 |

| Angle of attack (degree) | Velocity (m/s) | Lift(N) | Drag (N) |
|---|---|---|---|
| **10°** | 12.86 | .53 | .1 |
| | 18.20 | .96 | .2 |
| | 22.30 | 1.69 | .31 |
| | 25.75 | 1.88 | .34 |
| | 28.79 | 2.44 | .49 |
| | 31.54 | 2.91 | .67 |
| **15°** | 12.86 | .42 | .19 |
| | 18.20 | .95 | .38 |
| | 22.30 | 1.31 | .55 |
| | 25.75 | 1.86 | .52 |
| | 28.79 | 2.33 | .89 |
| | 31.54 | 2.67 | 1.15 |

| Angle of attack (degree) | Velocity (m/s) | Lift(N) | Drag (N) |
|---|---|---|---|
| **20°** | 12.86 | .45 | .28 |
| | 18.20 | .86 | .53 |
| | 22.30 | 1.35 | .78 |
| | 25.75 | 1.87 | 1.14 |
| | 28.79 | 2.32 | 1.43 |
| | 31.54 | 2.79 | 1.75 |
| **25°** | 12.86 | .44 | .35 |
| | 18.20 | .92 | .71 |
| | 22.30 | 1.13 | 1.01 |
| | 25.75 | 1.85 | 1.46 |
| | 28.79 | 2.31 | 1.85 |
| | 31.54 | 2.86 | 2.16 |

| Angle of attack (degree) | Velocity (m/s) | Lift(N) | Drag (N) |
|---|---|---|---|
| **30°** | 12.86 | .47 | .4 |
| | 18.20 | .95 | .79 |
| | 22.30 | 1.43 | 1.18 |
| | 25.75 | 1.9 | 1.57 |
| | 28.79 | 2.35 | 2 |
| | 31.54 | 2.8 | 2.48 |
| **35°** | 12.86 | .5 | .48 |
| | 18.20 | .92 | .9 |
| | 22.30 | 1.39 | 1.46 |
| | 25.75 | 1.86 | 1.99 |
| | 28.79 | 2.25 | 2.51 |
| | 31.54 | 2.84 | 3.03 |

| Angle of attack (degree) | Velocity (m/s) | Lift(N) | Drag (N) |
|---|---|---|---|
| **40°** | 12.86 | .46 | N/A |
| | 18.20 | .89 | N/A |
| | 22.30 | 1.36 | N/A |
| | 25.75 | 1.76 | N/A |
| | 28.79 | 2.15 | N/A |
| | 31.54 | 2.56 | N/A |
| **45°** | 12.86 | .39 | N/A |
| | 18.20 | .88 | N/A |
| | 22.30 | 1.23 | N/A |
| | 25.75 | 1.63 | N/A |
| | 28.79 | 1.99 | N/A |
| | 31.54 | 2.35 | N/A |

**Table A-4: Calculated velocity at different manometric head**

| (ΔH) $H_2O$ | Velocity (m/s) |
|---|---|
| **10** | 12.86 |
| **20** | 18.20 |
| **30** | 22.30 |
| **40** | 25.75 |
| **50** | 28.79 |
| **60** | 31.54 |

# Appendix B

**Graph B-1: Lift Vs. Angle of attack at 12.86m/s for different bird's wing.**

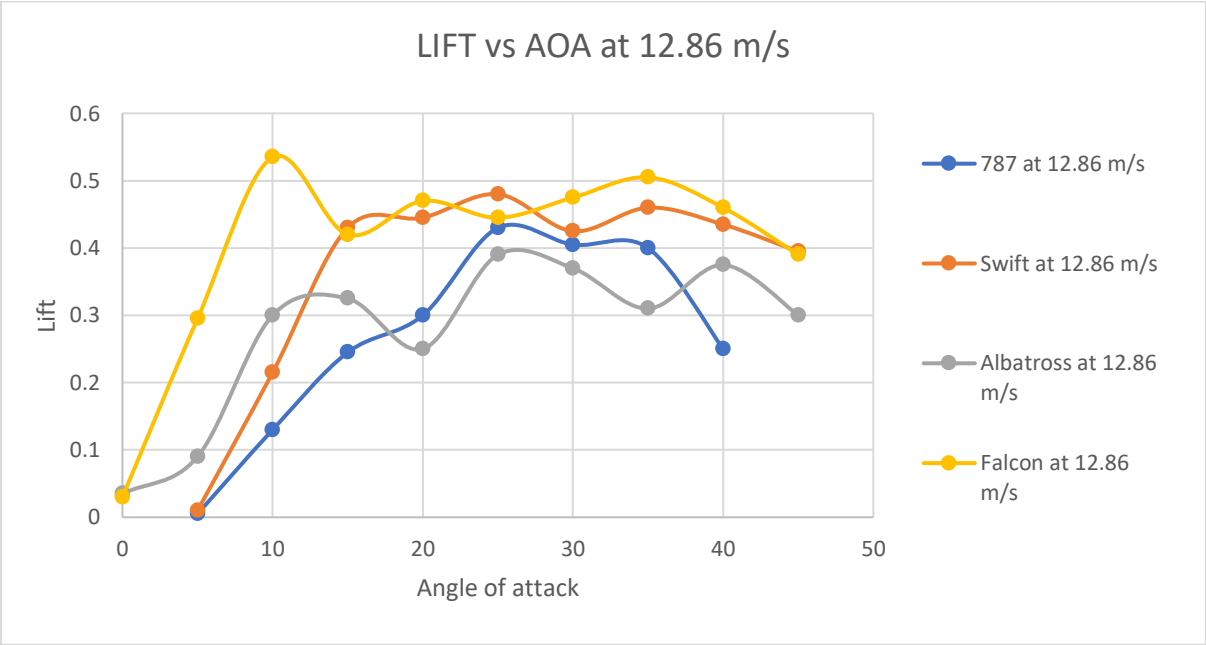


**Graph B-2: Lift Vs. Angle of attack at 18.20 m/s for different bird's wing.**

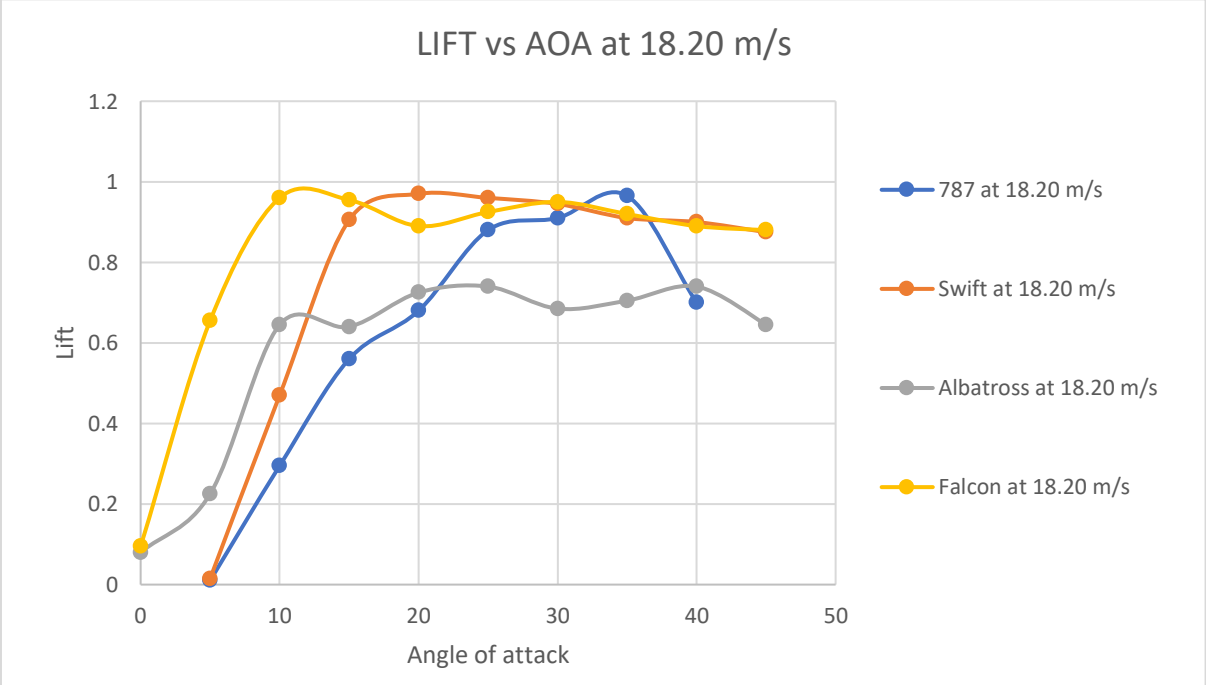

**Graph B-3: Lift Vs. Angle of attack at 22.30 m/s for different bird's wing**

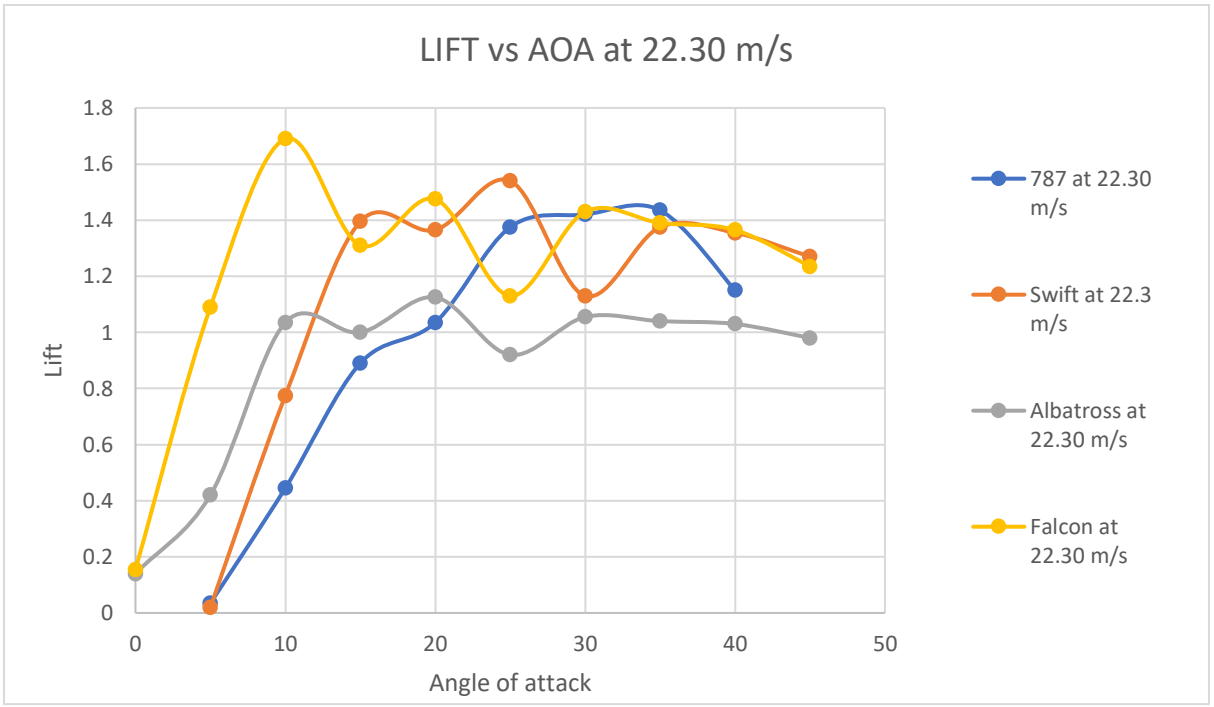


**Graph B-4: Lift Vs. Angle of attack at 25.75 m/s for different bird's wing**

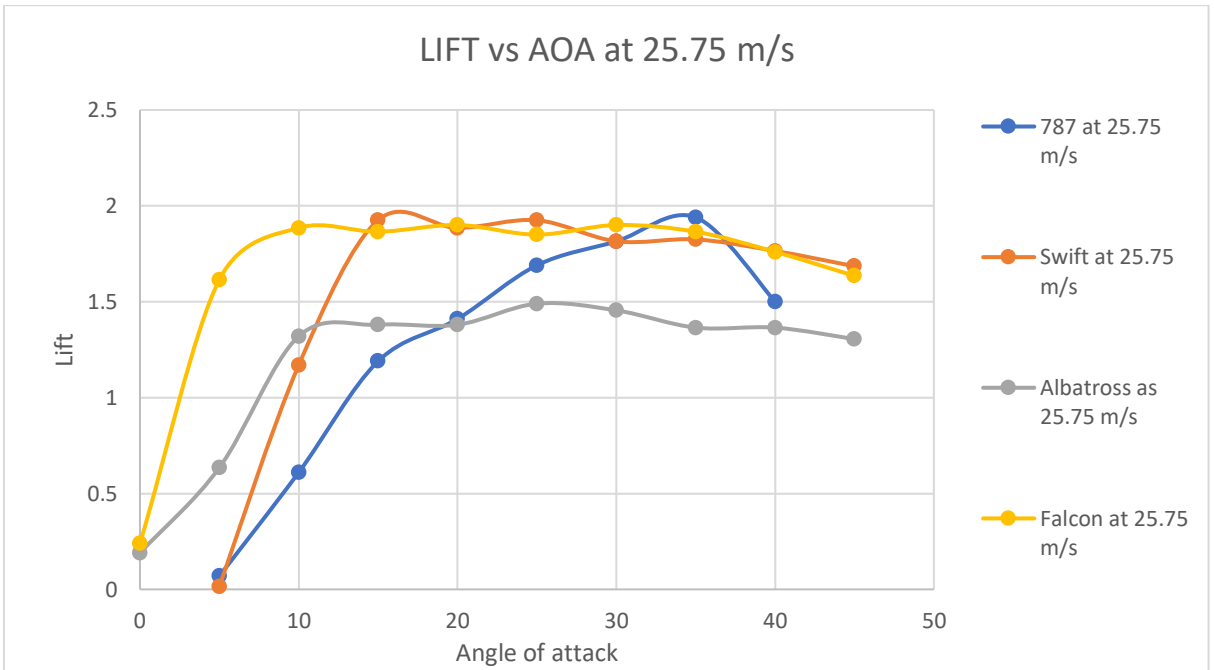

**Graph B-5: Lift Vs. Angle of attack at 28.79 m/s for different bird's wing.**

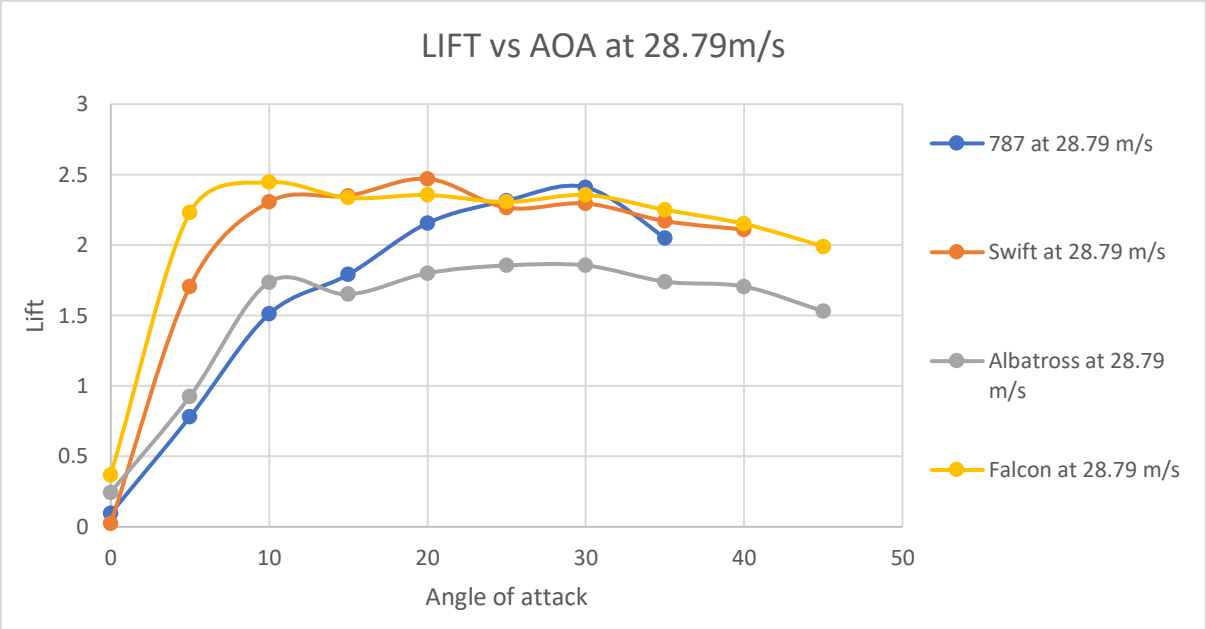


**Graph B-6: Lift Vs. Angle of attack at 31.54 m/s for different bird's wing.**

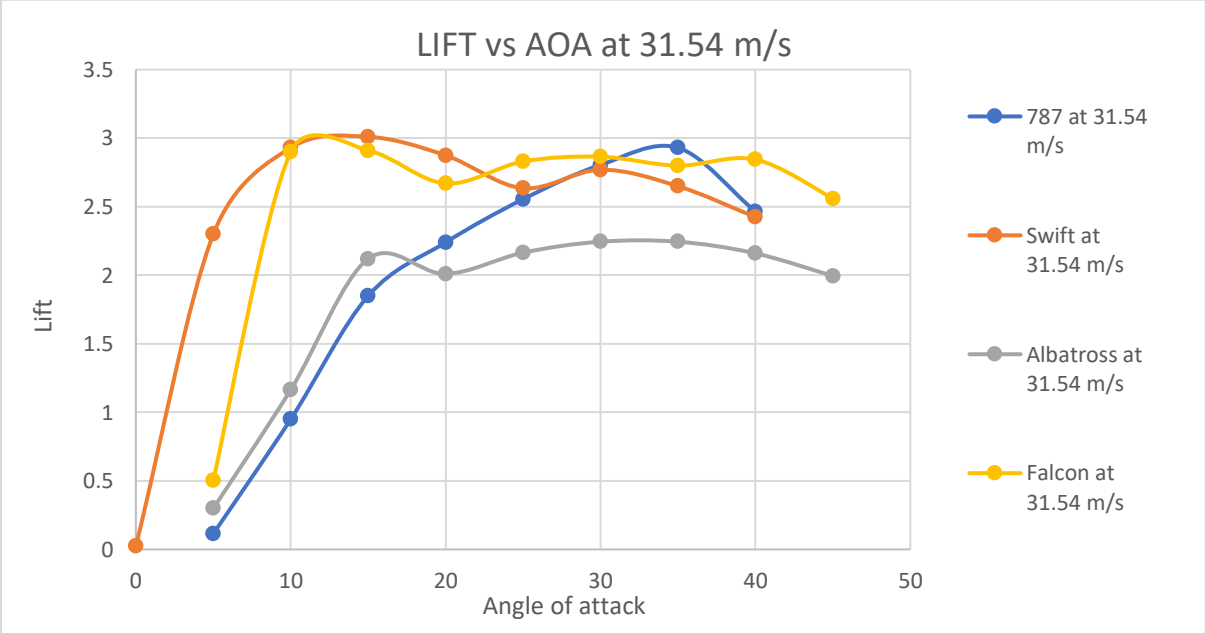

**Graph B-7: Drag Vs. Angle of attack at 12.86m/s for different bird's wing.**

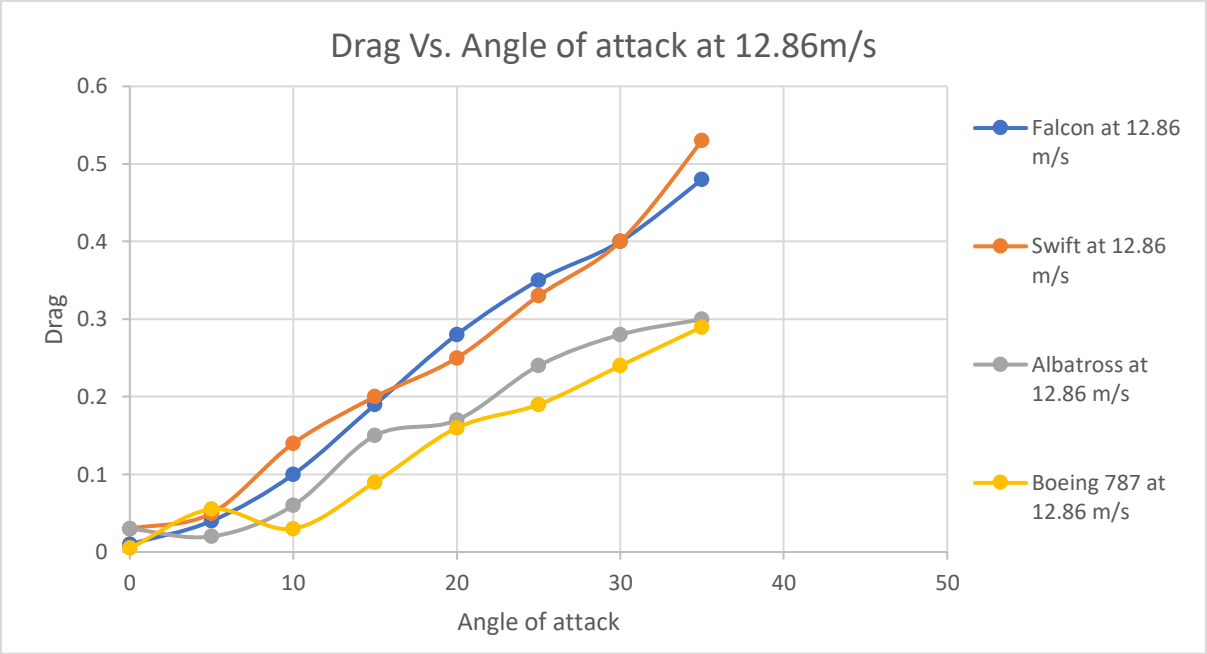


**Graph B-8: Lift Vs. Angle of attack at 18.20 m/s for different bird's wing.**

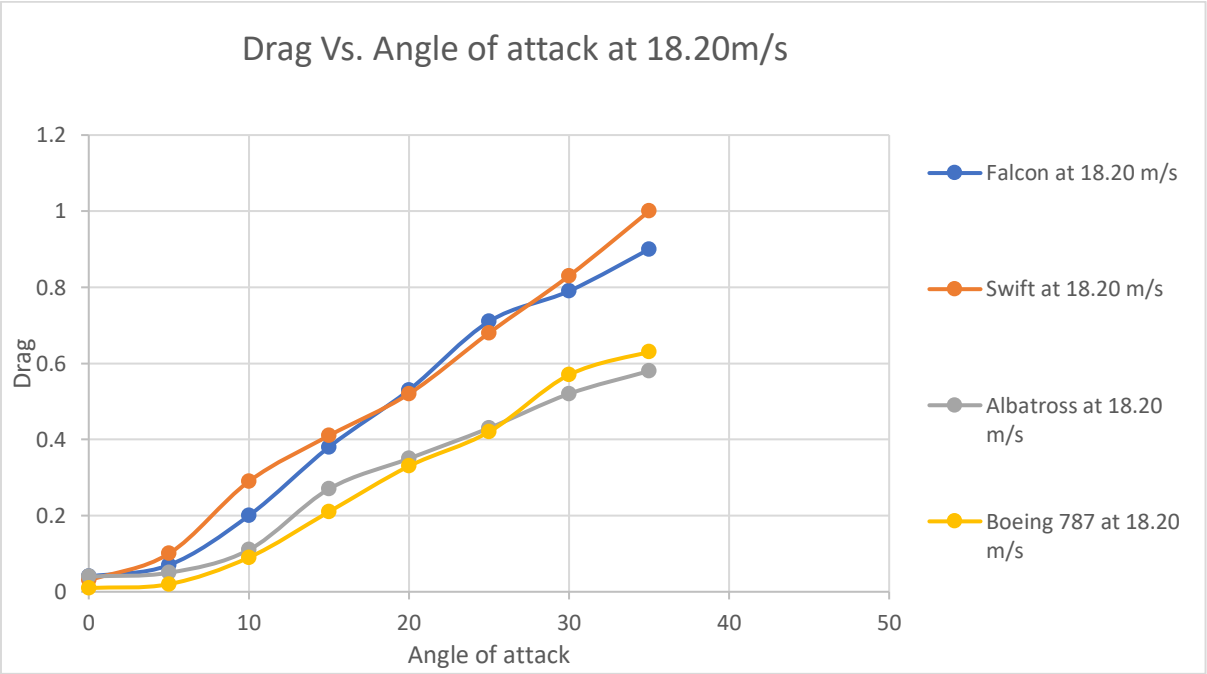

**Graph B-9: Drag Vs. Angle of attack at 22.30m/s for different bird's wing.**

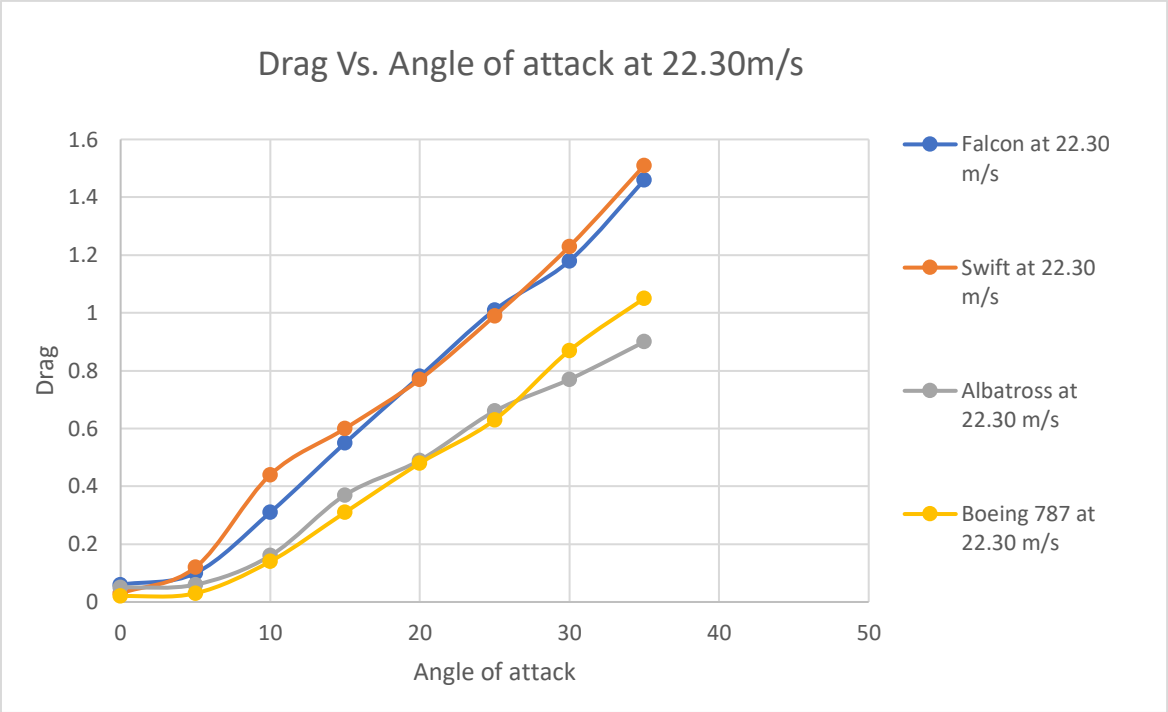


**Graph B-10: Drag Vs. Angle of attack at 25.75 m/s for different bird's wing.**

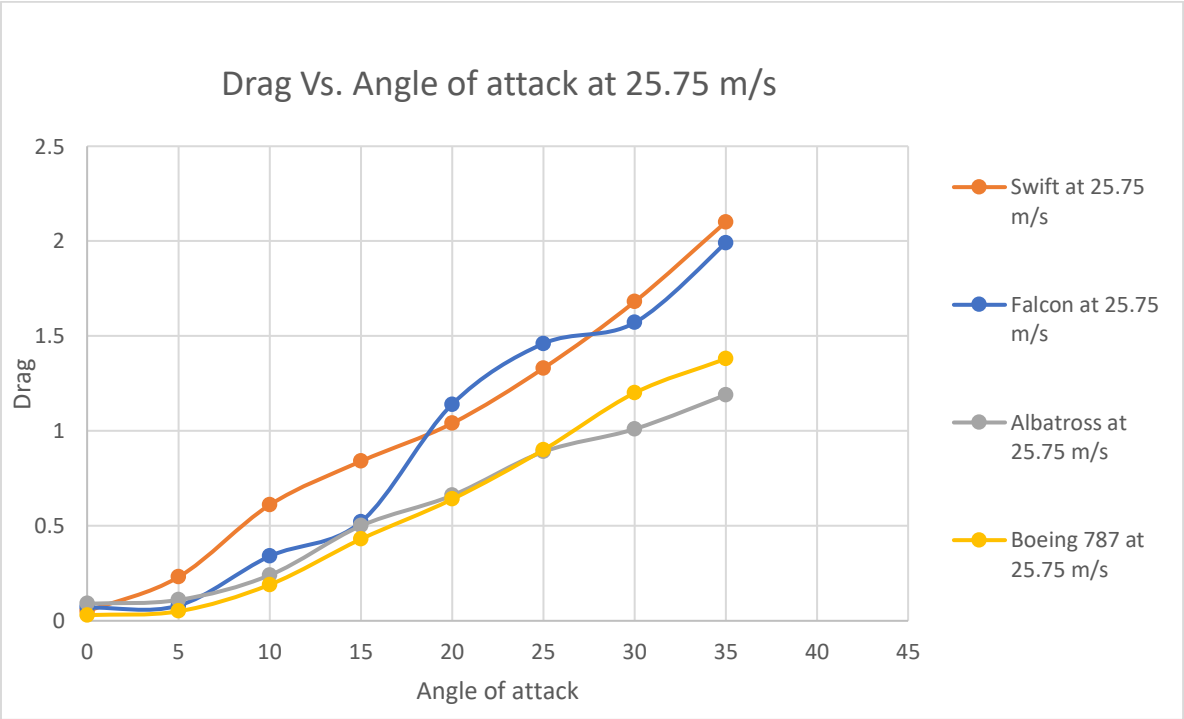

**Graph B-11: Drag Vs. Angle of attack at 28.79 m/s for different bird's wing.**

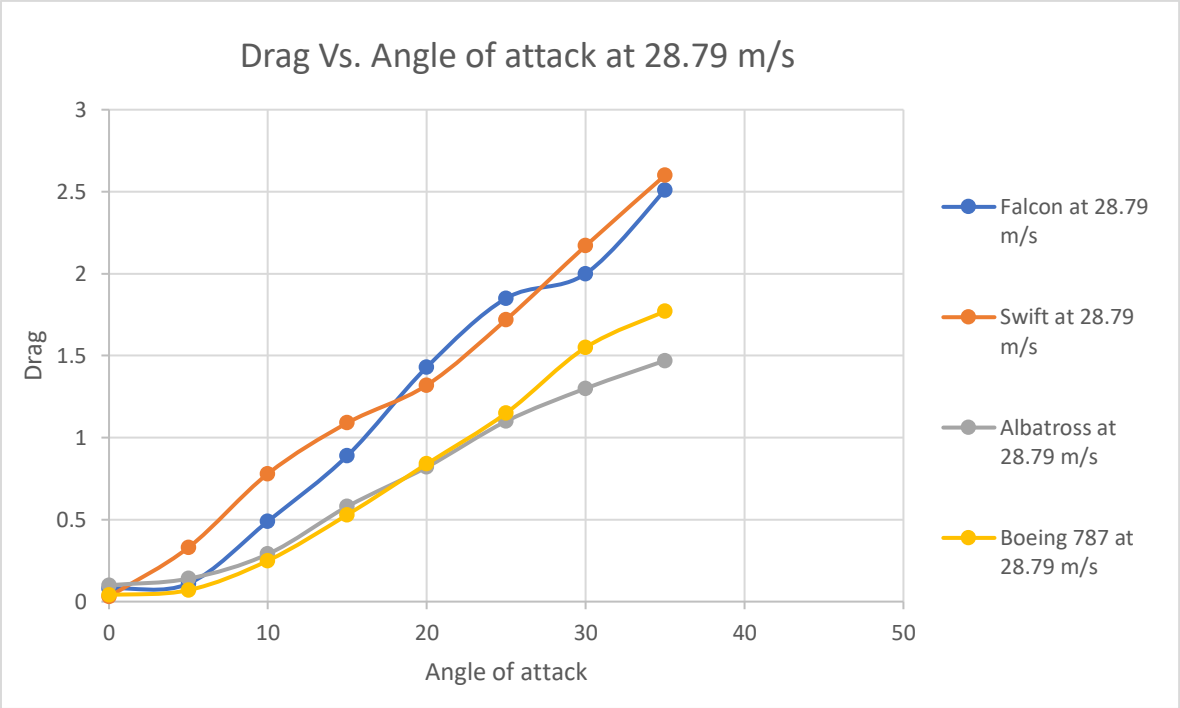


**Graph B-12: Drag Vs. Angle of attack at 31.54 m/s for different bird's wing.**

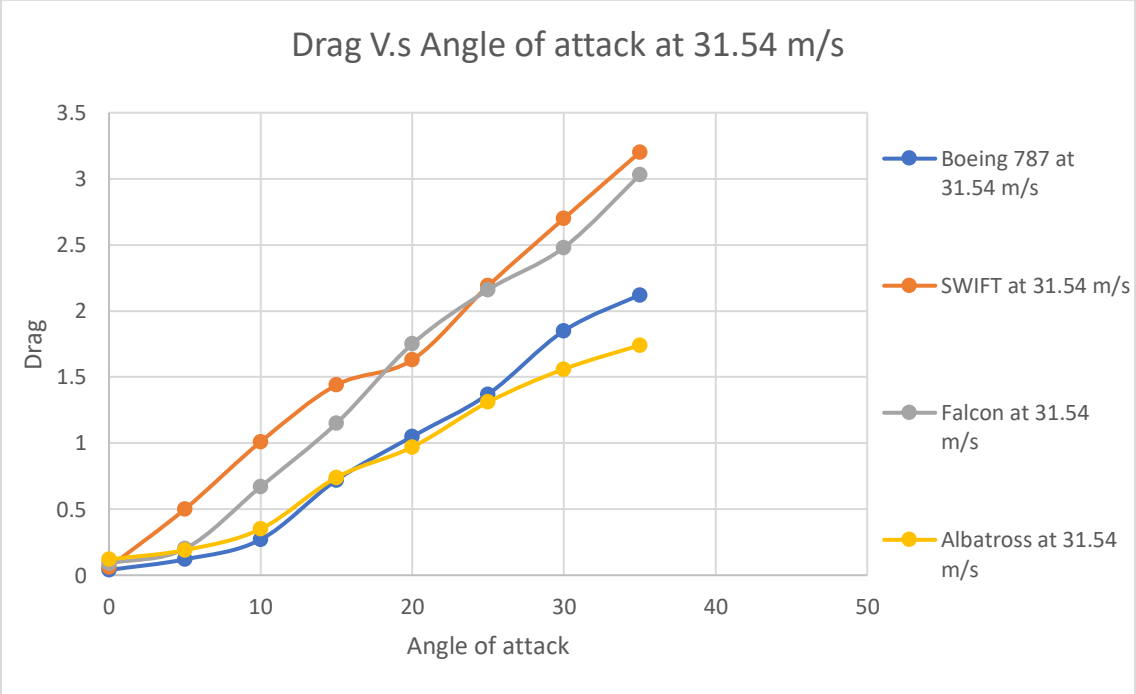

# Appendix C

**Figure C-1: Mesh view of Boeing 787-800**

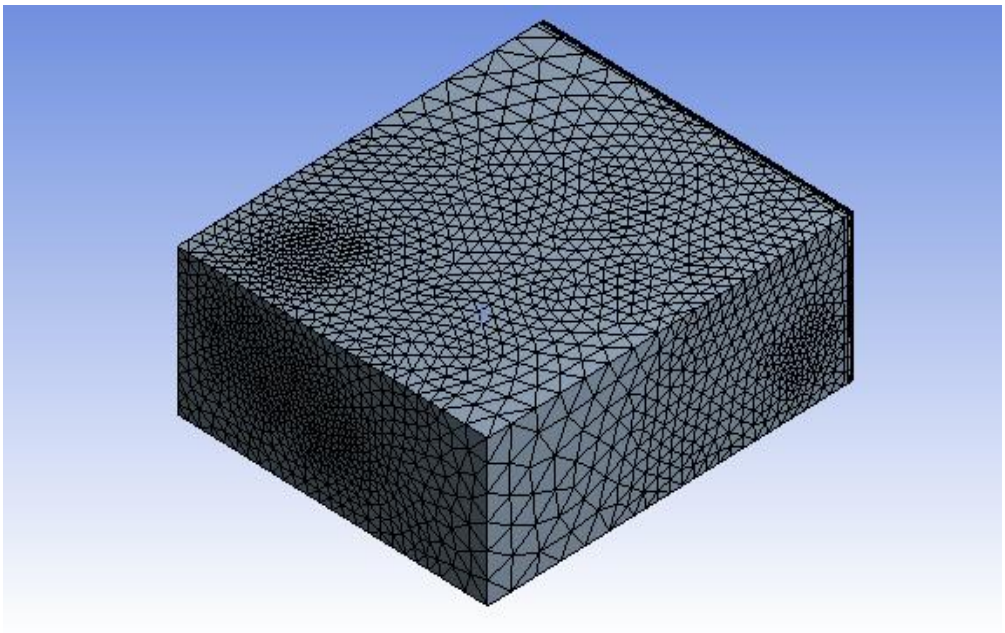

**Figure C-2: Pressure contour on Boeing 787-800 wing**

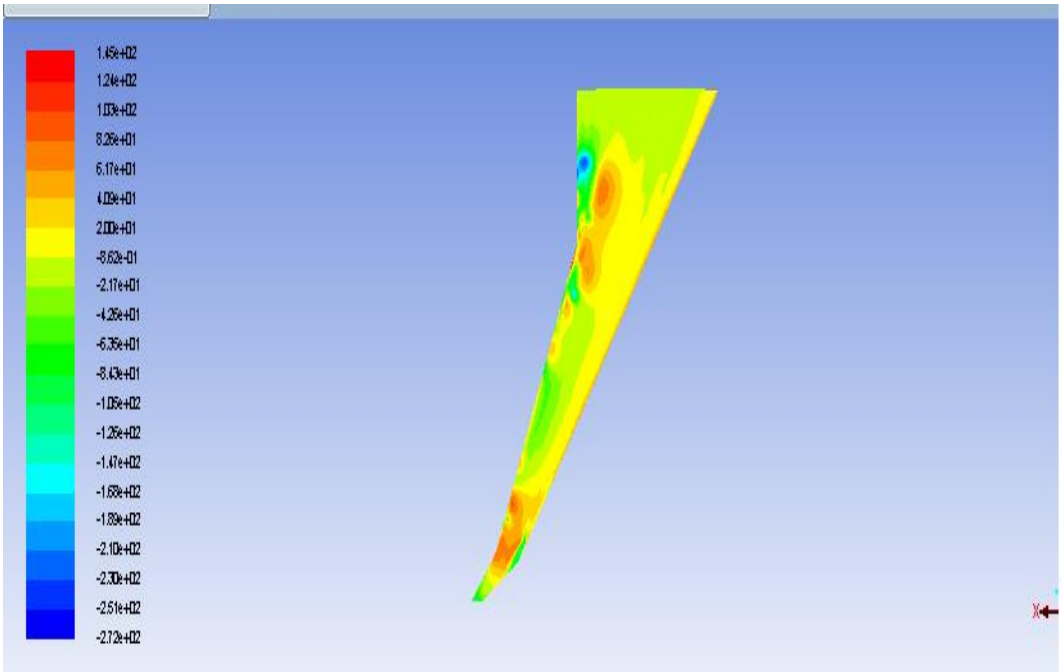

**Figure C-3: Velocity Streamline on Boeing 787-800 wing**

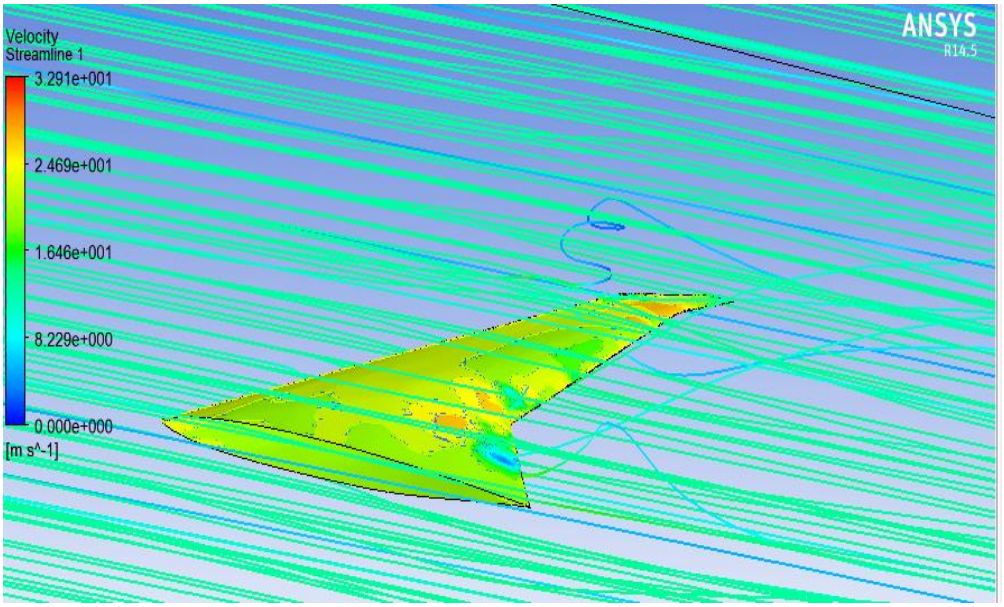


**Figure C-4: wireframe meshed view of Falcon wing inside computational domain**

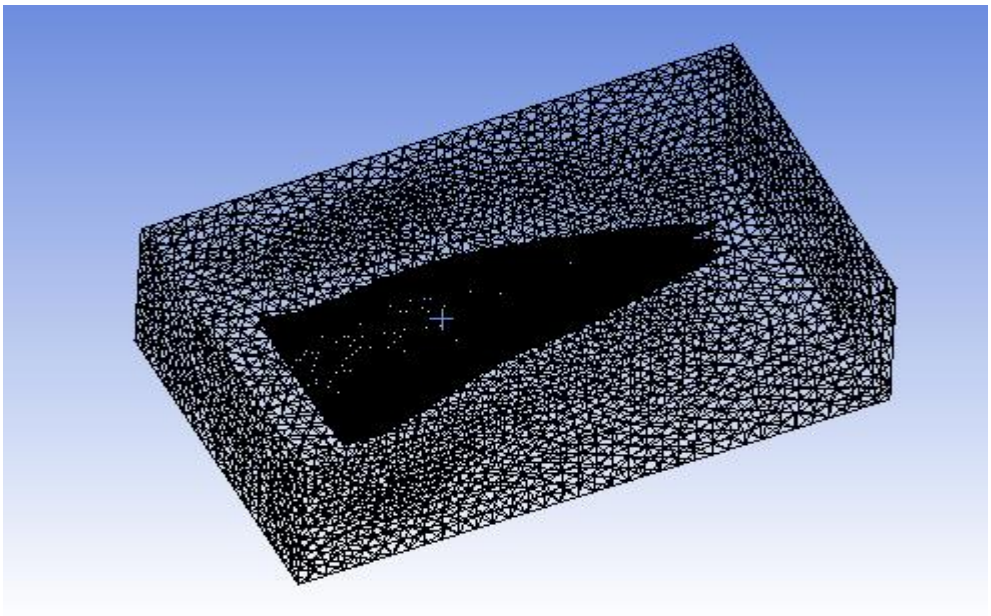

**Figure C-5: Pressure contour on Falcon wing**

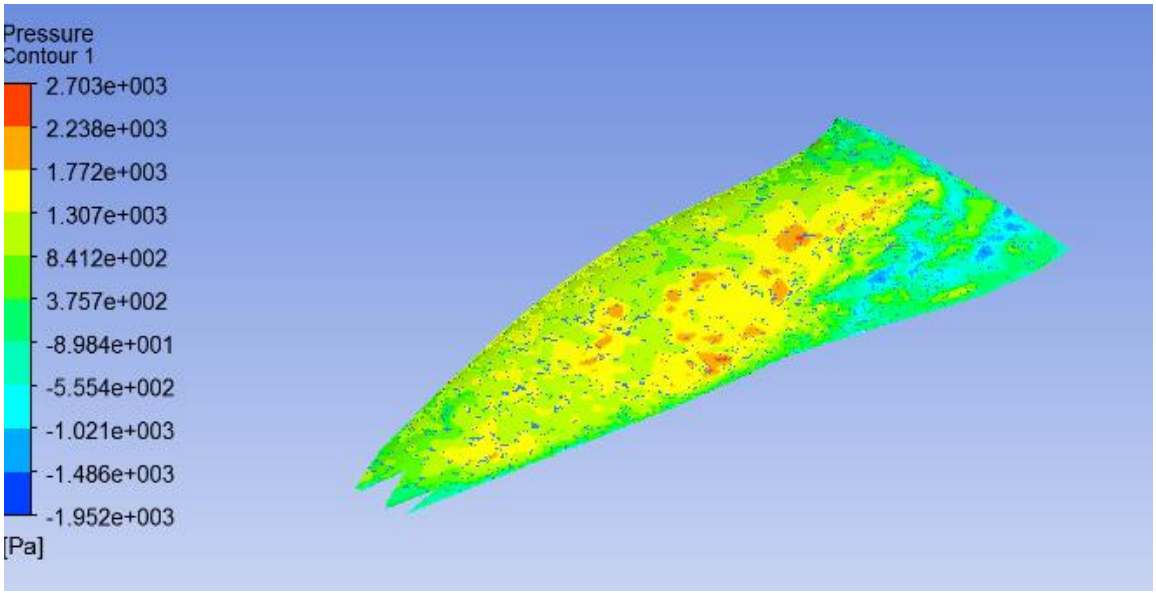


**Figure C-6: Stream line on Falcon wing**

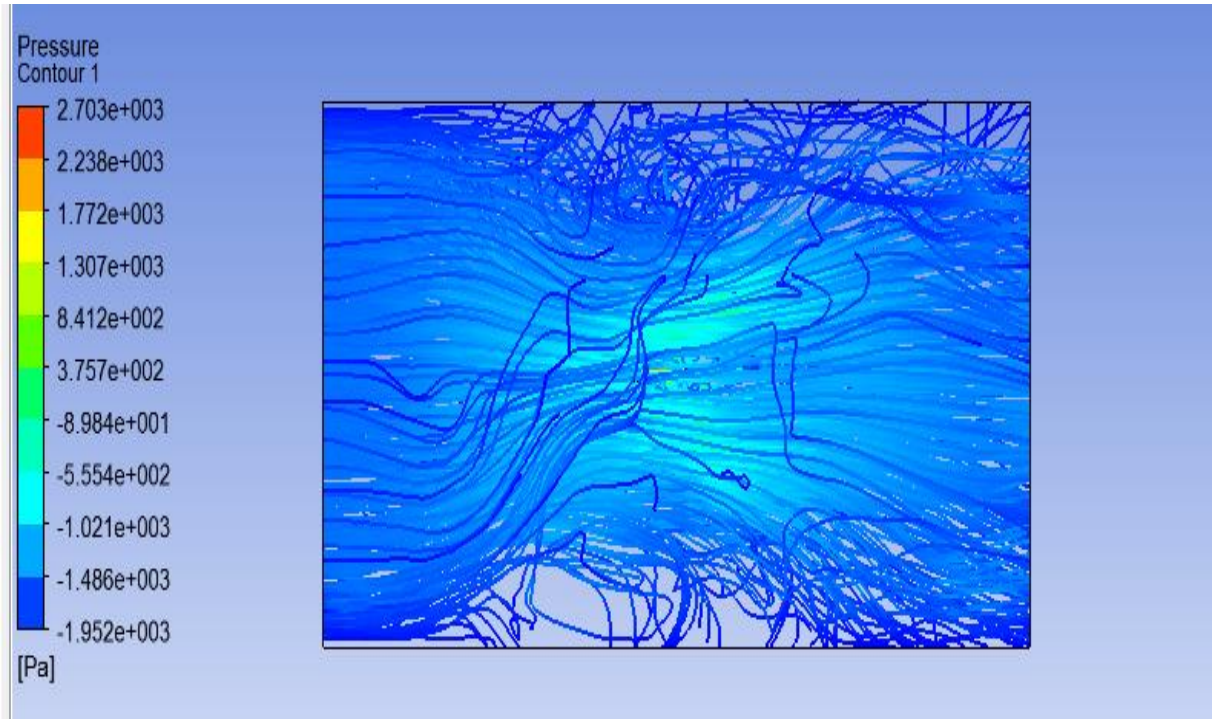

**Figure C-7: Wireframe meshed view of Swift wing inside computational domain**

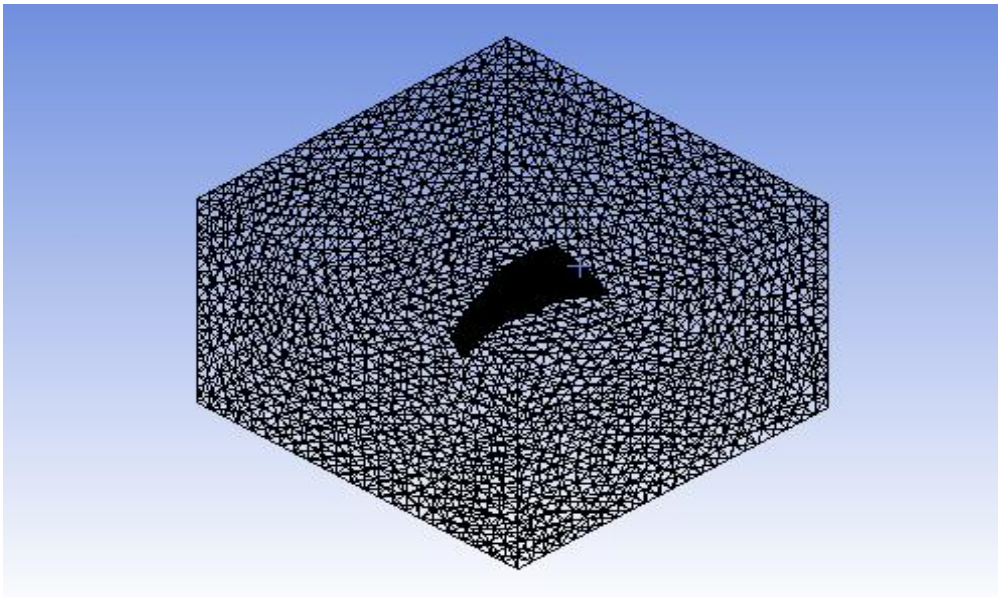

**Figure C-8: Pressure contour on Swift wing**

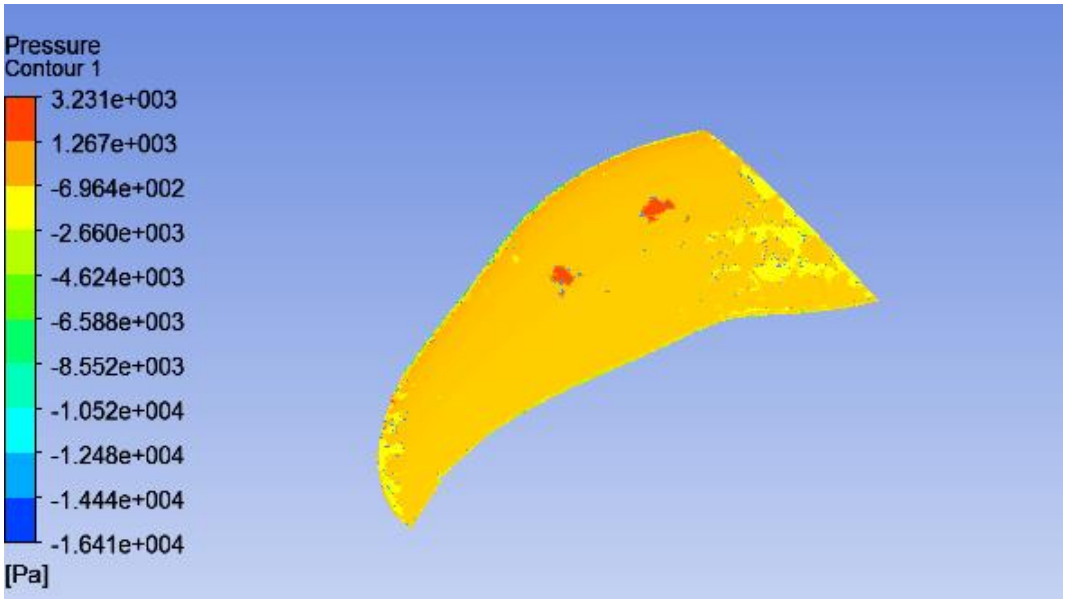

**Figure C-9: Albatross wing at 15-degree angle of attack**

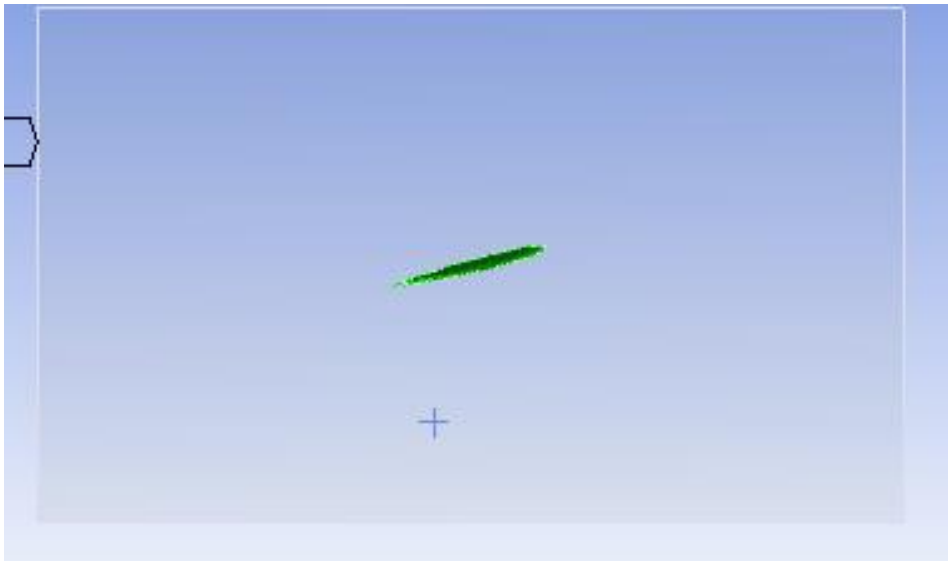

**Figure C-10: Albatross wing at the Centre of computational domain**